



Universiteit  
Leiden  
The Netherlands

## Cell-autonomous and host-dependent CXCR4 signaling in cancer metastasis : insights from a zebrafish xenograft model

Tulotta, C.

### Citation

Tulotta, C. (2016, June 14). *Cell-autonomous and host-dependent CXCR4 signaling in cancer metastasis : insights from a zebrafish xenograft model*. Retrieved from <https://hdl.handle.net/1887/40160>

Version: Not Applicable (or Unknown)

License: [Licence agreement concerning inclusion of doctoral thesis in the Institutional Repository of the University of Leiden](#)

Downloaded from: <https://hdl.handle.net/1887/40160>

**Note:** To cite this publication please use the final published version (if applicable).

Cover Page



Universiteit Leiden



The handle <http://hdl.handle.net/1887/40160> holds various files of this Leiden University dissertation.

**Author:** Tulotta, C.

**Title:** Cell-autonomous and host-dependent CXCR4 signaling in cancer metastasis : insights from a zebrafish xenograft model

**Issue Date:** 2016-06-14

# Chapter 5

## **CXCR4 signaling in the tumor microenvironment orchestrates experimental metastasis formation by controlling myeloid cell motility and response to malignant cells**

**Tulotta C., Stefanescu C., Torraca V., Meijer A.H. and  
Snaar-Jagalska B.E**

Institute of Biology, Leiden University, Gorlaeus Laboratories,  
Einsteinweg 55, 2333 CC, Leiden, the Netherlands

**Manuscript in preparation**

**Key words:** CXCR4, tumor microenvironment, neutrophils, macrophages,  
cancer metastases, zebrafish xenograft

## Abstract

Developing tumors constantly interact with the surrounding microenvironment. Myeloid cells exert both anti- and pro-tumor signals and chemokines are known to drive immune cell migration towards cancer cells. CXCR4 signaling supports tumor metastasis formation in tissues where CXCL12, its cognate ligand, is abundant. On the other hand, the role of neutrophilic and macrophagic CXCR4 signaling in driving cancer invasion and metastasis formation is poorly understood. Here, we use the zebrafish xenotransplantation model to unravel mechanisms underlying the function of CXCR4 in driving the interaction between invasive human tumor cells and host myeloid cells, supporting early metastasis formation. We found that experimental micrometastases fail to form in zebrafish mutant larvae lacking a functional *Cxcr4b*, generally highly expressed by myeloid cells. *Cxcr4b* controls neutrophil development, motility and interaction with cancer cells and guides macrophage recruitment to metastatic sites. Using RNA sequencing technology, we found that motility and adhesive gene expression signatures are differentially altered in neutrophils and macrophages, FACS-sorted from *Cxcr4b*-deficient zebrafish larvae. In conclusion, we propose that CXCR4 signaling supports the interaction between tumor and myeloid cells in developing tumor. Therefore, targeting CXCR4 on tumor and myeloid cells in patients affected by metastatic neoplasia could serve as a double bladed razor to limit cancer progression.

## 5

## Introduction

Tumor-microenvironment interactions are crucial in cancer pathogenesis and several signals drive this communication [1]. The composition of the cancer microenvironment changes in different stages of cancer progression [2]. Fibroblasts, endothelial and immune cells are main components of the tumor stroma, acting in concert with the extracellular matrix (ECM), growth factors, proteases and cytokines [3]. The CXCR4-CXCL12 chemokine signaling pathway sustains tumor cell growth and directs the formation of distant metastases. It is established that cancer cells expressing CXCR4 home to secondary organs where CXCL12 is highly secreted, mainly by mesenchymal stromal cells [4]. Moreover, CXCL12 guides the migration of stromal cells that express CXCR4 and locally infiltrate the tumor, providing support by secretion of growth and angiogenic factors, as well as promoting metastasis through activation of epithelial-to-mesenchymal transition (EMT) via MAPK, PI3K/Akt and NF $\kappa$ B pathways [3, 5].

A dual role in either supporting or inhibiting tumor progression has been linked with the immune system [1]. CXCR4-CXCL12 signaling has been associated with the polarization towards an immune-suppressive microenvironment: the possible role of a CXCL12 shield that protects cancer cells from being recognized by cytotoxic lymphocytes and activates regulatory T-cells has recently been described [6]. Polarization of macrophages towards a M2 phenotype has also been associated with tumor survival. Differentiation of macrophages into classically activated-M1 or alternatively activated-M2 types is

directed by the balance of cytokine-associated signals, present in the tissue [7]. In an inflammatory state, macrophages display a Toll-like- and IFN $\gamma$ - induced M1 phenotype, characterized by production of pro-inflammatory cytokines, like IL1 $\beta$ , IL6, TNF $\alpha$ , and parallel to a Th1-type response from the adaptive immune system [7] [8]. On the other hand, tissue repair, angiogenesis and resolution of inflammation require macrophage activation towards a M2 type, guided by IL4 and IL13 (Th2 cytokines), resulting in the production of anti-inflammatory cytokines (IL10) and activation of a Th2-type adaptive response, with recruitment of T regulatory cells to limit the immune response [7] [8].

Colony-stimulating factor 1 (CSF1)-Colony stimulating factor receptor 1 (CSFR1) guides the attraction of macrophages towards tumorigenic sites and regulates macrophage and tumor cell streaming towards blood vessels, initiating cancer cell intravasation [9]. Moreover, tumor-associated-macrophages (TAMs) are also recruited to the tumor site via CCL2 and support tumor angiogenesis via secretion of vascular endothelial growth factor (VEGF), platelet-derived growth factor (PDGF), tumor growth factor (TGF $\beta$ ) and CXCL8 [9]. Recent studies have pointed at the role of perivascular CXCR4-expressing M2 macrophages in creating tumor vascular networks after chemotherapy, leading to tumor relapse, and confirmed CXCR4 as M2 marker [10]. In analogy to macrophages, neutrophils have also been classified in N1 (antitumoral) and N2 (protumoral) types [11-13]. The polarization of neutrophils towards one or the other type is driven by a plethora of cytokines and chemokines that often direct the same polarization in macrophages. In particular, pro-inflammatory molecules such as IFN $\beta$ , IL1 $\beta$  and TNF $\alpha$  induce the polarization towards type 1 phenotypes, while IL10 and TGF $\beta$  are immunosuppressive and inhibitory of inflammation, skewing neutrophil polarity towards N2. Pro-tumoral and pro-angiogenic N2 neutrophils express high levels of VEGF, MMP9 and CXCR4 [13].

Macrophages and neutrophils have been reported to display overlapping as well as complementary functions in infection and tumor relapse after chemotherapy [14, 15]. Interestingly, tissue-resident macrophages, originated from the fetal liver during embryo development, and monocyte-derived macrophages, originated from HSPCs in the adult bone marrow, work in concert to regulate recruitment of neutrophils in inflamed tissues, through epithelial layers [16]. Recent findings suggest that neutrophils and macrophages work together to regulate the hematopoietic niche [17]. The bone microenvironment represents a favorable site of metastatic growth for different tumor types, suggesting a possible involvement of the signals that regulate bone marrow and hematopoietic niche homeostasis [18]. Among those, CXCR4-CXCL12 signaling is a major candidate, considering its fundamental role in orchestrating HSPC and neutrophil retention in and mobilization from the bone marrow, with the involvement of the CXCL1/CXCL2-CXCR2 chemokine axis [19-21].

The use of the zebrafish embryo as a xenotransplantation model has shown that hematogenously inoculated tumor cells home in the caudal hematopoietic tissue (CHT), where tumor growth and invasion take place, initiating early metastatic events [22] (Chapter 4). The CHT is an intermediate site of hematopoiesis during zebrafish

embryogenesis and is the functional analogue of the fetal liver in mammalian development [23]. Previous work from our group has suggested the role of neutrophils in preparing the metastatic niche by non-pathological transmigration from the CHT to the tail fin and *vice versa*. In their random motility, neutrophils form paths in the collagen, favoring tumor cell invasion [22]. Here, we address the role of the host-dependent CXCR4 signaling in driving the communication between tumor and myeloid cells during experimental metastasis formation in an *in vivo* zebrafish xenogeneic model.

## Results

### Myeloid cells support early metastatic events of triple negative breast cancer

Immune cells play dual roles during cancer progression. Inhibitory and supportive functions of the immune system have been associated with tumor growth and metastasis formation. Using the zebrafish embryo model we previously showed that myeloid cells, mainly neutrophils, support the establishment of tumor experimental micrometastasis, when the MAE-FGF2 transformed cell line was inoculated into the blood circulation of 2-day-old embryos [22]. Therefore, we used the same approach to investigate whether zebrafish myeloid cells would exert similar tumor supportive functions, when other cell lines were implanted. In particular, we used the osteotropic triple negative breast cancer line MDA-MB-231-B, derived from bone metastases formed in a mouse xenograft model [24]. The zebrafish embryo model bears the great advantage of studying the contribution of the innate immune system during early metastasis formation separately from the adaptive immunity, which reaches full maturity in 3-4 week old juveniles [25]. To deplete both neutrophils and macrophages, we injected Pu.1/Spi1b morpholino (1 mM) into 1-2 cell stage embryos. Subsequently, the MDA-MB-231-B cell line was inoculated into the blood circulation of 2 days post fertilization (dpf) zebrafish embryos with GFP-expressing neutrophils. The reporter line *Tg(mpx:GFP)<sup>114</sup>* [26] was used to monitor neutrophil depletion, in view of the time-limited efficacy of gene knock-down obtained with morpholino anti-sense oligos. Macrophage depletion was not monitored as it already occurs with lower doses of the same morpholino (0.5 mM). Tumor phenotype assessment was performed 2 days post implantation (dpi) by quantifying tumor cell invasion in each larva. Depletion of myeloid cells in the Pu.1 morphants resulted in a reduced cancer cell invasion (68%), in the tail fin in proximity of the caudal hematopoietic tissue (CHT) (Figure 1). As previously found, the CHT, a site of hematopoiesis and analogous to the fetal liver during mammalian development, is a preferential site of early cancer metastasis formation in the zebrafish xenotransplantation model. In conclusion, myeloid cells support triple negative breast cancer early metastasis onset in zebrafish.

### CXCR4 signaling in myeloid cells is involved in early tumor metastasis initiation

Therapeutic targeting of CXCR4 on tumor cells could be an effective strategy to limit tumor cell growth and metastasis. However, CXCR4 signaling in the tumor

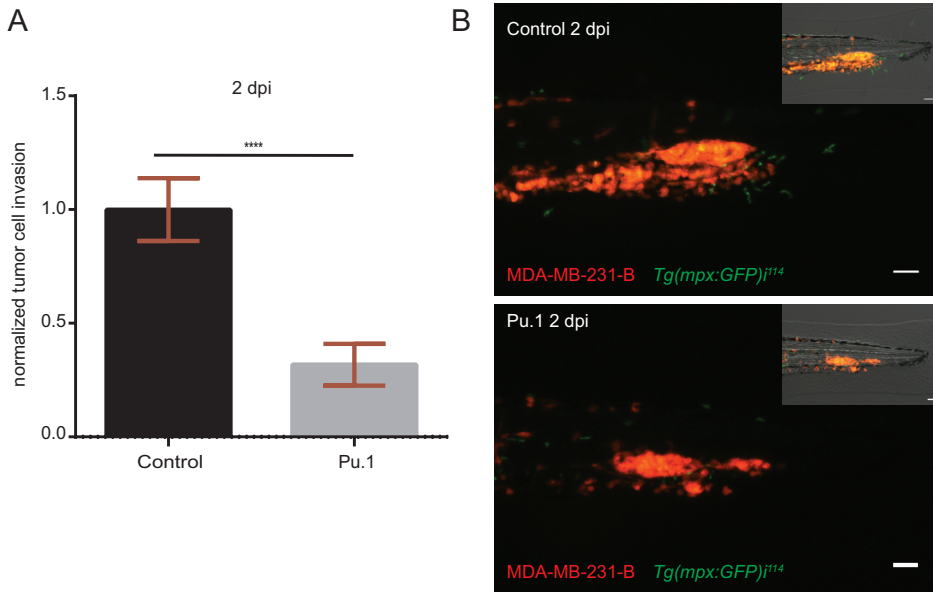


**Figure 1. Myeloid cell depletion impairs tumor cell invasion.** (A) Relative tumor invasion was compared at 2 dpi in Pu.1 morphants, depleted of neutrophils and macrophages, and larvae injected with control morpholino (68% inhibition). Two-tailed un-paired t-test with Welch's correction (\*\*\*\* $p < 0.0001$ ) was performed on a pool of two biological replicates (Control:  $n=84$ , Pu.1:  $n=67$ ). Data are mean $\pm$ SEM. (B) Top panel shows MDA-MB-231-B cells forming a tumor mass and invading the tail fin tissue (bright field image, top right), while surrounded by GFP expressing neutrophils in 2 dpi *Tg(mpx:GFP)<sup>114</sup>* injected with a control morpholino. In the bottom image, neutrophils are absent due to Pu.1 knockdown and a smaller tumor mass is formed compared to the control condition, resulting in impaired invasion of the local tissue (bright field, top right). Scale bar: 50  $\mu$ m. Micrographs were acquired using a Leica MZ16FA fluorescent microscope coupled to a DFC420C camera.

microenvironment also plays a central role in cancer and further investigations are needed to fully understand its contribution.

In our model, teleost evolution has led to a *cxc4* gene duplication. *cxc4a* and *cxc4b* paralogues are expressed by different cell types, although redundant functions have been reported [27]. We performed transcriptome analysis of FACS-sorted neutrophils and macrophages from 5 dpf *Tg(mpx:GFP)<sup>114</sup>* and *Tg(mpeg1:EGFP)<sup>g22</sup>* larvae, respectively, and RNA deep sequencing revealed very high expression levels of the *cxc4* paralogues in neutrophils and macrophages, confirming data published by others on different stages of embryo development [28]. In particular, *cxc4a* and *cxc4b* transcriptomic levels were higher in the GFP<sup>+</sup> fractions compared to the GFP<sup>-</sup> populations. Importantly, *cxc4b* levels were at least 100-fold higher than *cxc4a* levels in both myeloid cell types, indicating that *cxc4b* is the predominant human CXCR4 orthologue in the zebrafish larval immune cells (Figure 2A). Therefore, to study if CXCR4 signaling in the tumor microenvironment supports cancer metastasis initiation, we engrafted the triple negative breast cancer cell line MDA-MB-231-B in the *cxc4b*<sup>t26035</sup> (*odysseus* or *ody*) mutant [29]. Xenogeneic transplantation into the blood circulation via the duct of

Cuvier resulted in a strong proliferating and invasive tumor phenotype, characterized by experimental micrometastasis formation in the CHT region in the wild-type (wt) siblings, whereas a significant reduction was observed in the *cxcr4b*<sup>-/-</sup>; *ody* mutants (Figure 2B-E). The establishment of early metastatic events defined by tumor mass formation and extravasation followed by local tissue invasion was monitored at 2 (Figure 2B-C) and 4 (Figure 2D-E) days after engraftment and tumor burden was found to be significantly inhibited in *ody* larvae (22.5% and 40.5% reduction at 2 and 4 dpi, respectively). In

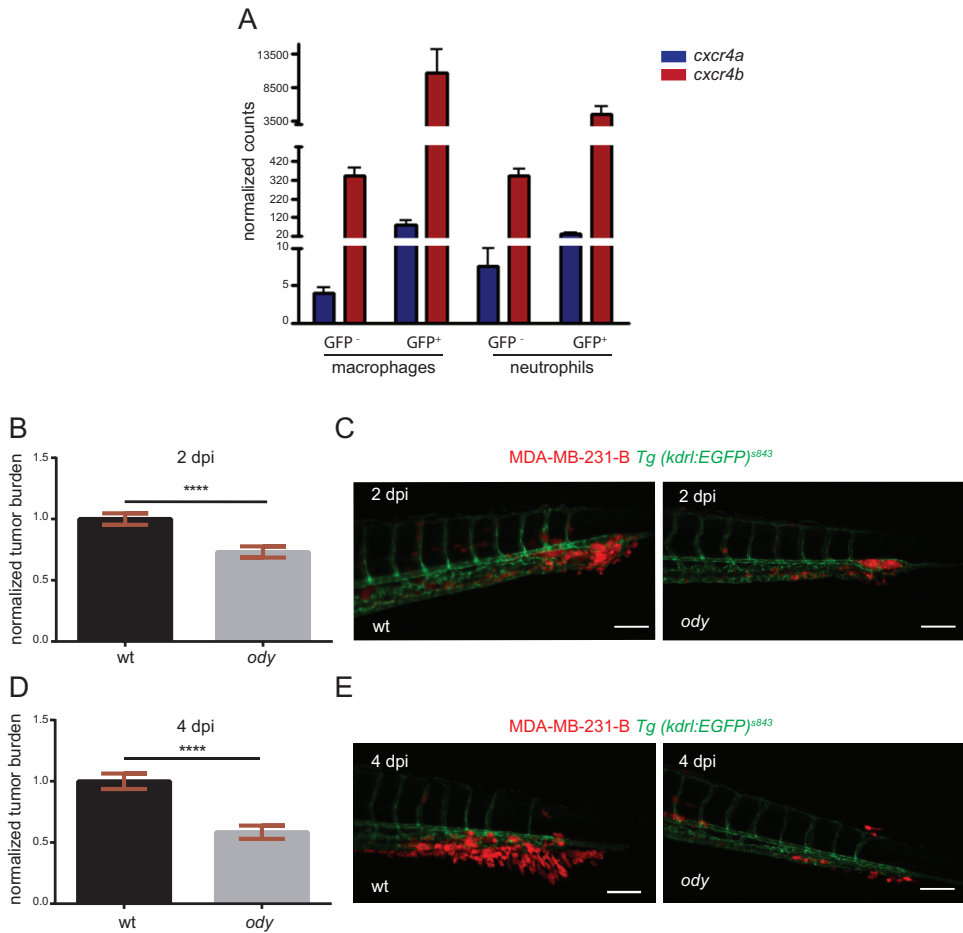


**Figure 2. *cxcr4b* is highly expressed in neutrophils and macrophages and loss of function results in reduced triple negative breast cancer burden.** (A) *cxcr4b* expression levels were quantified in neutrophils and macrophages and compared to the GFP negative cell population. Data are read counts from RNA sequencing performed on two biological replicates and show *cxcr4b* gene expression enrichment in both neutrophils (~10-fold) and macrophages (~30-fold), compared to GFP<sup>-</sup> cells in zebrafish larvae. FACS-sorted neutrophils were obtained from 5 dpf *Tg(mpx:GFP)<sup>1114</sup>* larvae, while FACS-sorted macrophages were derived from 5 dpf *Tg(mpeg1:EGFP)<sup>g122</sup>*. (B) Relative metastatic tumor burden of MDA-MB-231-B-DsRed cells was quantified in *ody* and wt siblings at 2 dpi. Data are mean ± SEM of two independent experiments (wt: n=64, *ody*: n=57). Un-paired t-test \*\*\*\*p<0.0001. (C) MDA-MB-231-B tumor cells establish a secondary tumor

mass, with initiation of single cell extravasation, in wt larvae, whereas a phenotype inhibition is found in *ody* mutants at 2 dpi (22.5% reduction). (D) MDA-MB-231-B tumor burden was measured in wt and *cxcr4b* null mutants at 4 dpi, at the metastatic site where secondary growth began at 2 dpi. A 40.5% reduction in tumor burden was observed. Data are mean  $\pm$  SEM of two independent experiments (wt: n=59, *ody*: n=43). Un-paired t-test, with Welch's correction \*\*\*\*p<0.0001. (E) Highly invasive cancer cells display aggressive and metastatic features in wt siblings, whereas few cells remain in the CHT region of 4 dpi *ody* larvae. Scale bars: 50  $\mu$ m. Micrographs are acquired using a Leica MZ16FA fluorescent microscope coupled to a DFC420C camera.

order to understand whether the *Cxcr4* signaling inhibition in the microenvironment could affect the metastatic cascade in other tumor types, we engrafted another triple negative breast cancer cell line MDA-MB-157 (Figure 3A-B), as well as prostate cancer cells PC3-M-Pro4-Luc2 (Figure 3C-D). Tumor early metastasis establishment in the CHT region of 4 dpi zebrafish larvae was impaired in the *ody* mutant line compared to the wt siblings, when each cell line was inoculated into the blood circulation (reduction of tumor burden was 52%, and 38% in breast and prostate tumor cell lines, respectively) (Figure 3). Therefore, we suggest that the host *Cxcr4* signaling, prevalent in neutrophils and macrophages, plays a crucial role in the early steps of metastases formation of triple negative breast cancer as well as other tumor types.

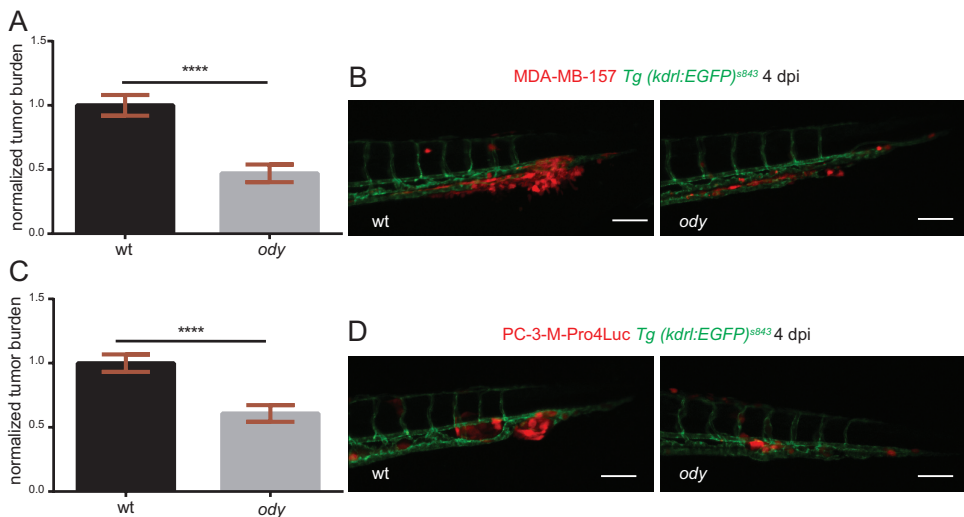


**Figure 3. *cxcr4b* deficient host microenvironments block metastatic burden of breast and prostate cancer cells.** (A) Metastatic burden was assessed in 4 dpi zebrafish larvae engrafted with the triple negative breast line MDA-MB-157 mCherry. A 52% reduction was found. Data are mean  $\pm$  SEM of two independent experiments (wt: n=42, *ody*: n=28). Un-paired t-test, with Welch's correction \*\*\*\*p<0.0001. (B) Secondary tumor mass, extravasation and invasion fail to occur in *ody* mutants compared to wt siblings. (C) A significantly lower tumor burden in *cxcr4b* deficient larvae was observed when the prostate cancer PC3-M-Pro4-Luc2 mCherry or td-tomato cell line was implanted (38% reduction). Data are mean  $\pm$  SEM of two independent experiments (wt: n=48, *ody*: n=46). Un-paired t-test \*\*\*\*p<0.0001. (D) Prostate early metastasis formation, characterized by a solid tumor mass formation in the CHT region of zebrafish larvae, occurs in wt siblings and is significantly decreased when *Cxcr4b* signaling is impaired in the host. Scale bars: 50  $\mu$ m. Micrographs re acquired using a Leica MZ16FA fluorescent microscope coupled to a DFC420C camera.

## Cxcr4b signaling inhibition attenuates neutrophil basal motility and development

CXCR4 signaling has been found to play an important role in regulating neutrophil retention in the CHT in the WHIM syndrome, where neutropenia has been linked to increased susceptibility to infection in patients as well as in the zebrafish model [28, 30]. Therefore, as neutrophils express high levels of *cxcr4b*, we investigated whether the impairment of Cxcr4 signaling affects the motility of neutrophils in the CHT region, altering their ability to prepare the metastatic niche. Neutrophil migration under physiological conditions was assessed in 3 dpf zebrafish embryos, the same time point used in [22]. Interestingly, neutrophils displayed reduced motility when Cxcr4b signaling was impaired in the *ody* mutant compared to the wt siblings (Figure 4A-C).

During zebrafish development, primitive and definitive waves of hematopoiesis can be distinguished. In a transition phase, between 24 and 36 hpf, neutrophils originate from the posterior blood island (PBI), which, with the onset of the definitive wave, is replaced by the CHT [31] (Figure 4D). Recent studies in zebrafish have revealed that CXCR4 signaling has a direct link with the development of hematopoietic stem and progenitor cells (HSPCs), mainly affecting their ability to colonize the CHT, which functions as an intermediate hematopoietic site [32]. In the same study, the use of the CXCR4 antagonist AMD3100, between 48 and 72 hpf, decreased *cmyb/runx*<sup>+</sup> HSPCs numbers. Because neutrophils develop first in the PBI, independently from the HSPCs, and subsequently develop in the CHT, dependently on the HSPCs with self-renewal potential, we investigated whether the development of neutrophils could be affected in a host with a non-functional Cxcr4b signaling. Neutrophil number was quantified during earlier stages of development (1 dpf), before HSPCs colonize the CHT and initiate the definitive wave of hematopoiesis. An increase in neutrophil number was found in the CHT of *ody* embryos, compared to wt siblings, whereas no difference was detected on whole embryo level (Figure 4E-G). Subsequently, neutrophil number was quantified in the whole zebrafish embryo, as well as in the CHT region, in between the dorsal aorta and caudal vein, starting from the end of the yolk extension, in 2 and 6 day old *cxcr4b*<sup>-/-</sup> and *cxcr4b*<sup>+/+</sup> *Tg (mpx:GFP)*<sup>114</sup> embryos. To verify neutrophil number, the time points 2 and 6 days post fertilization were chosen as correspondent to the time points of cancer cell engraftment and metastasis formation assessment, respectively. We identified an increase (31%) in neutrophil number in the CHT region of *ody* mutants compared to wt siblings (Figure 4H-I) at 2 dpf. At the same time, no difference in total neutrophil number was observed (Figure 4J). Interestingly, neutrophil number decreased in the CHT of *ody* mutants compared to wt siblings at 6 dpf (Figure 4K-L). Moreover, at the same time point, the overall number of neutrophils was found to be lower (Figure 4M). These findings suggest a potential effect of Cxcr4b in regulating both HSPCs-independent and HSPCs-dependent neutrophil development. In the second case, our results are in line with the altered ability of HSPCs to colonize the CHT and interact with the surrounding stroma in the presence of CXCR4 antagonist [32].

In conclusion, *Cxcr4b* signaling impairment affects neutrophil motility and development, in a time dependent-manner, suggesting different functions of this chemokine signaling axis during neutrophil development before and after HSPC-dependent hematopoiesis.

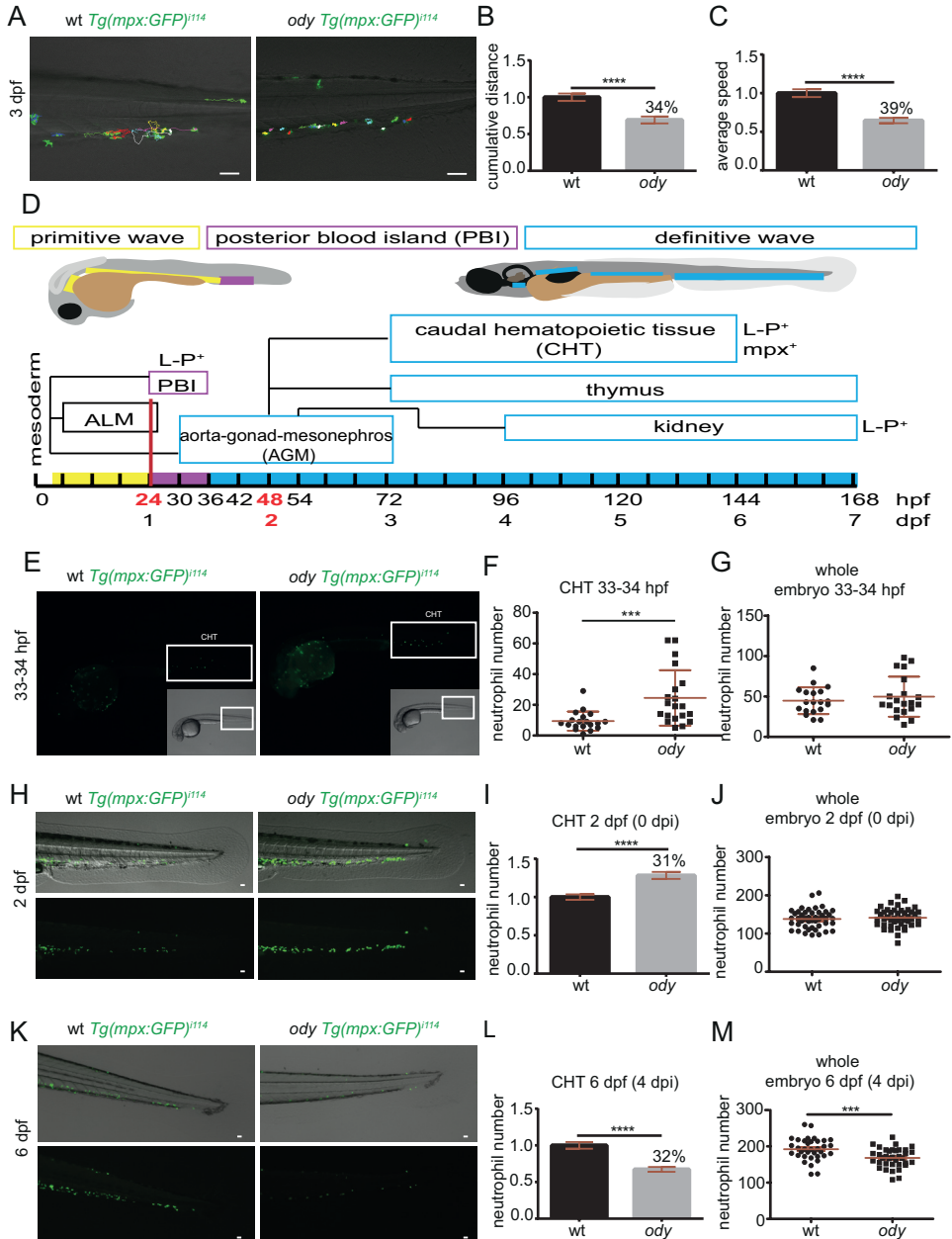


**Figure 4. *cxcr4b* deficiency affects neutrophil physiological motility and development.** (A) Neutrophil movement was recorded for 30 minutes and tracks show reduced motility in *ody* compared to wt siblings in the tail fin region where tumor metastasis formation generally takes place. Scale bars: 50  $\mu$ m. Time-lapse microscopy was performed using a Leica TCS SPE confocal microscope with a HC APO 20x DRY objective (0.7 N.A.). Neutrophil motility was assessed in wt and *ody* larvae at 3 dpf, measuring cumulative distance (B) and average speed (C) of each phagocyte, localized in the CHT region. (B) Un-paired t-test \*\*\*\*  $p < 0.0001$  and (C) Un-paired t-test, with Welch's correction \*\*\*\*  $p < 0.0001$ . Data are mean  $\pm$  SEM of two independent experiments and values were calculated from 54 tracks (wt: n=7) and 58 tracks (*ody*: n=8). (D) Scheme of hematopoiesis, adapted from [31]. As in other vertebrates, two waves of hematopoiesis, primitive and definitive, occur in zebrafish. During the primitive wave, myelopoiesis takes place in the anterior lateral mesoderm. When the blood circulation begins (24 hpf, red line), the hematopoiesis transiently shifts to the posterior blood island (PBI). Here, hematopoietic progenitor cells have multi-lineage potential and give rise to the erythromyeloid progenitors, from which endothelial and myeloid cells form. The definitive hematopoiesis begins from the aorta-gonad-mesonephros (AGM). AGM progenitor cells enter the blood circulation around 33 hpf. By 48 hpf, hematopoietic stem and progenitor cells (HSPCs), with long-term and self-renewal potentials, migrate to the CHT and kidney marrow and seed the thymus by 54 hpf. L-P (L-Plastin) is a myeloid cell marker and mpx myeloperoxidase is a neutrophil marker. (E-G) Neutrophil number was counted in wt and *ody* siblings at 33-34 hpf, when neutrophil development is independent from HSPC colonization of the CHT, indicated by the box (E). (F) A significantly higher number of neutrophils is present in the *ody* embryos in the CHT region, compared to wt siblings, while the total neutrophil number was found unchanged in *cxcr4b*<sup>+/+</sup> and *cxcr4b*<sup>-/-</sup> (G). Data are mean  $\pm$  SD. Mann-Whitney test \*\*\*  $p < 0.0004$ . In (F) and (G) n=19 (wt) and n=20 (*ody*). (H, I) Neutrophils are counted in wt and *ody* mutants in the site of hematopoiesis (CHT) at 2 dpf and a significant increment is registered in *ody* embryos (31% increase) (H, top panel is a bright field image of bottom panel showing GFP<sup>+</sup> neutrophils; I, data quantification). (I) Un-paired t-test, with Welch's correction \*\*\*\*  $p < 0.0001$ . Data are mean  $\pm$  SEM of two independent experiments (wt: n=47, *ody*: n=45). (J) Total neutrophil number is counted in wt and *ody* mutants at 2 dpf and no difference is found. In (J) wt: n=45, *ody*: n=45. (K, L) Number of neutrophils in wt and *ody* in the CHT region at 6 dpf is shown. A lower neutrophil number was found in the CHT region in *cxcr4b*<sup>-/-</sup> larvae (32% reduction), as shown by top and bottom micrographs (K) and quantified in (L). Un-paired t-test \*\*\*\*  $p < 0.0001$ . Data are mean  $\pm$  SEM of two independent experiments (wt: n=35, *ody*: n=36). (M) A significant reduction in total neutrophil number is present in *ody* larvae during later developmental stages. In (M) wt: n=35, *ody*: n=36. Data are mean  $\pm$  SEM (pool of two independent experiments). Un-paired t-test \*\*\*  $p = 0.0007$ .

### **Cxcr4b signaling affects the neutrophilic response towards cancer cells during early metastasis formation**

Considering the involvement of Cxcr4b signaling in driving neutrophil motility and development under basal conditions, we investigated next whether the ability of neutrophils to respond to cancer cells was affected in the *ody* mutant. Generally, emergency hematopoiesis is initiated upon systemic infections and neutrophils leave the bone marrow in response to damage and danger signals, during inflammation and infection [33-36]. Emergency hematopoiesis, dependent on gcsf-gcsfr signaling, has also been shown to occur in zebrafish larvae, resulting in expansion of HSPCs and mobilization of neutrophils from the CHT in response to lipopolysaccharide (LPS) injection [37] or bacterial infection [38]. Hence, the number of neutrophils in the CHT was quantified  $\sim$  3-6 hours after MDA-MB-231-B tumor cells were inoculated into the blood circulation of embryos at 2 dpf. We found that the acute response of neutrophils to tumor cell engraftment was characterized by a decreased number of neutrophils in the CHT in the wt siblings, compared to the uninjected control. The same response was found in the *ody* embryos: in comparison with uninjected *ody* larvae, the presence of tumor cells in the dorsal aorta, caudal vein and branched vessels of the CHT plexus

led to a decrease in neutrophil number in the CHT, and no differences were found with the tumor-engrafted wt siblings (Figure 5A-B). These results suggest that, at 2 dpf, the mobilization of neutrophils from the CHT in response to tumor engraftment is independent from *Cxcr4b*. As tumor early metastatic events in the CHT region were primarily affected in *ody* mutants at 4 dpi and the CHT colonization by HSPCs is known to occur at 2 dpf, the neutrophil response to cancer cells was also assessed at 4 dpi (6 dpf). Like in 2 dpf embryos, we also observed a reduction of neutrophil numbers in the CHT of tumor-engrafted wt siblings at 6 dpf, compared to the uninjected controls. In contrast, neutrophil numbers were unchanged in tumor-engrafted *ody* mutants, compared to uninjected *ody* larvae (Figure 5C-D). Simultaneously, MDA-MB-231-B cells were found to establish a tail fin invasive phenotype in the wt larvae, whereas reduced aggressive properties were observed in the *ody* mutants (Figure 5C, top panel), in agreement with our earlier observations (Figure 2). Therefore, contrary to the situation at 2 dpf, *Cxcr4b* signaling appears to be required for the mobilization of neutrophils from the CHT as well the the tumor-invasive phenotype at 6 dpf.

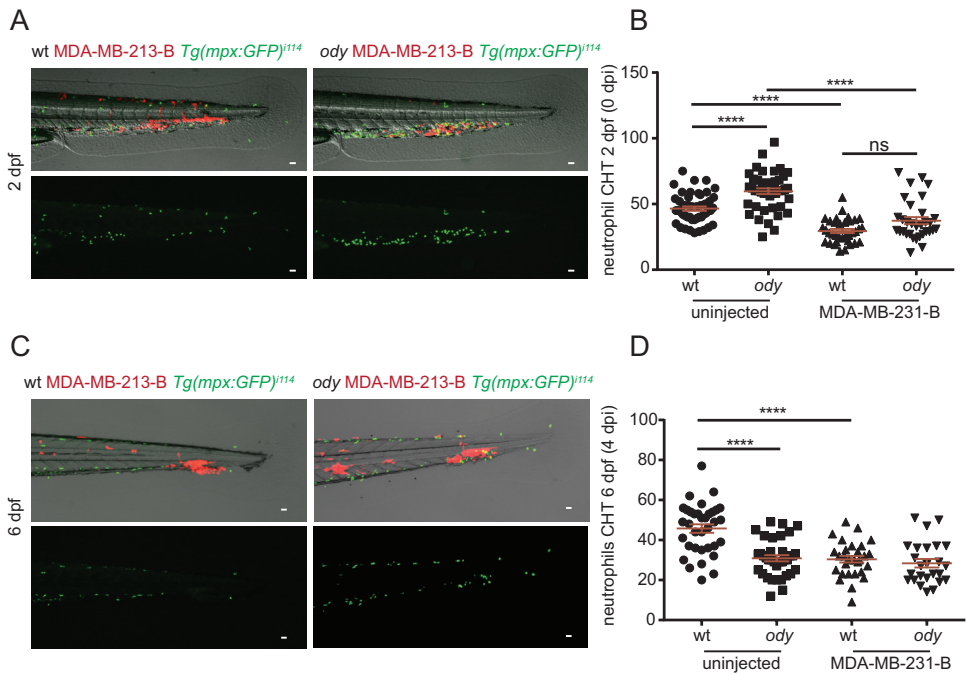


**Figure 5. *cxcr4b* loss of function influences the neutrophil response to cancer cells initiating early metastases.** (A, B) Neutrophil response to cancer cells ~3-6 hours after engraftment in the blood circulation of 2 dpf zebrafish embryos, wt or *ody* mutant, in a *Tg(mpx:GFP)<sup>114</sup>* background. (A, top panel is an overlay of bright field, DsRed<sup>+</sup> and GFP<sup>+</sup> channels and corresponds to the bottom panel where only GFP<sup>+</sup> neutrophils are shown). (B) Neutrophils exit the CHT in response to tumor cells, both in the wt and *ody* embryos. Kruskal-Wallis, with Dunn *post hoc* test \*\*\*\*  $p < 0.0001$ , ns  $p > 0.05$  (number of uninjected embryos is the same as in graph in Figure 4I; number of engrafted embryos is wt: n=35 and *ody*: n=32). (C, D) The neutrophil response to tumor metastatic niche formation was assessed by measuring neutrophil number in the CHT in wt and *ody* larvae at 4 dpi (6 dpf). In control conditions, neutrophils leave the CHT when

tumor cells are present, whereas they fail to respond, remaining in the CHT, in *ody* mutants as shown in the image panel in (C) and quantified in (D). Kruskal-Wallis, with Dunn *post hoc* test \*\*\*\*  $p < 0.0001$  (number of uninjected embryos is the same as in graph in Figure 4L; number of engrafted embryos is wt:  $n=29$  and *ody*:  $n=25$ ). All images were acquired using Leica MZ16FA fluorescent microscope coupled to a DFC420C camera. Scale bars: 50  $\mu\text{m}$ .

To further support the evidence that neutrophils display a different response towards cancer cells when *Cxcr4b* signaling is not functional, we quantified neutrophil motility in the metastatic region at 4 dpi (6 dpf). Neutrophils displayed a motility pattern characterized by lower speed and diminished average distance, in presence of MDA-MB-231-B in the wt siblings, compared to the uninjected controls (Figure 6A, B, E, F). On the other hand, no differences in neutrophil speed and travelled distance were detected in the *ody* siblings, either uninjected or implanted with MDA-MB-231-B (Figure 6C, D, E, F). In conclusion, *Cxcr4b* signaling impairment affects neutrophil development and response to cancer cells initiating early metastatic events. Moreover, the process occurs in a time-dependent manner and it is likely to be directly linked to the role of CXCR4 during hematopoiesis.

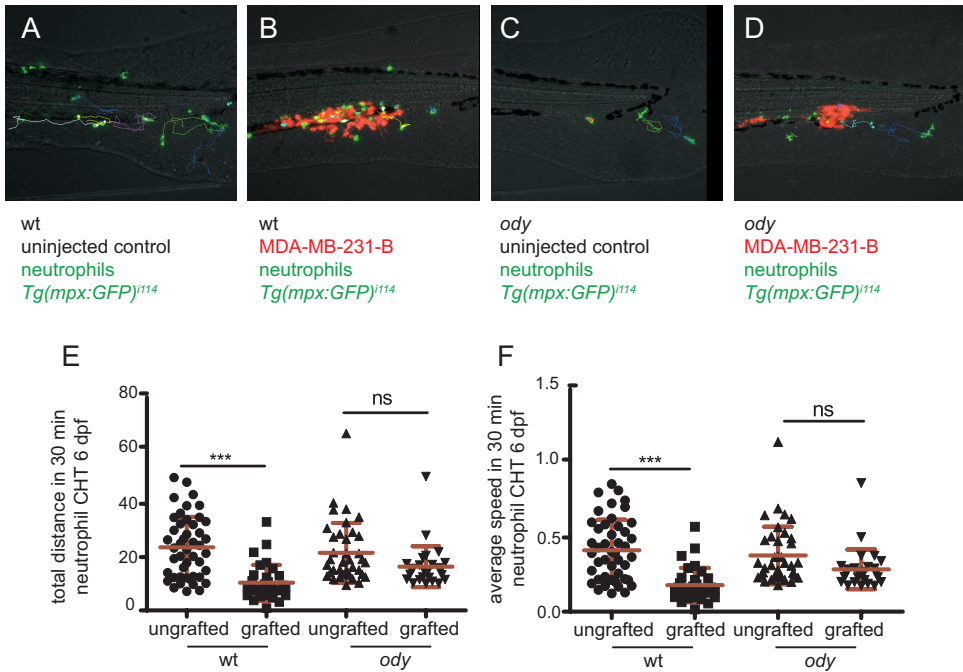


**Figure 6. Neutrophils display a different pattern of migration in response to metastatic tumor cells, in siblings bearing wt or mutated *cxcr4b*.** (A, B) Neutrophil tracking in 6 dpf larvae shows stationary behavior of neutrophils in the presence of tumor cells in the wt siblings compared to the uninjected controls. (C, D) Neutrophils maintain the same migratory behavior in *ody* mutants, in presence of MDA-MB-231-B and in uninjected larvae. (E, F) Neutrophil motility was quantified for 30 minutes, measuring total distance and average speed of each neutrophil in the CHT region. Data are mean $\pm$ SD (uninjected wt:  $n=46$  tracks from 7 larvae; MDA-MB-231-B wt:  $n=32$  tracks from 5 larvae; uninjected *ody*:  $n=37$  tracks from 7 larvae; MDA-MB-231-B *ody*:  $n=27$  tracks from 5 larvae). One-way ANOVA, with Bonferroni *post hoc* test.

## Cxcr4b regulates macrophage responses to early metastatic events

Having shown that Cxcr4b is required for the development of neutrophils and their response to metastatic events in our zebrafish model, we next investigated whether impairment of CXCR4 chemokine signaling in the host could affect the macrophage response to cancer cells. In order to test that, we first assessed the response of macrophages to cancer cells colonizing the CHT, after engraftment in the blood circulation of 2 day old *Tg(mpeg1:EGFP)<sup>g/22</sup>* zebrafish embryos. The number of macrophages (mpeg<sup>+</sup> cells) significantly increased in the surrounding of the CHT at 2 dpi, when MDA-MB-231-B tumor cells were present (Figure 7A-B), compared to the uninjected control group. A significantly higher number of macrophages could also be detected in the same metastatic region at 4 dpi, compared to uninjected larvae (Figure 7C-D), although the difference at this time point appeared lower than at earlier stages after engraftment.

Next, we investigated whether Cxcr4b signaling impairment affects the ability of macrophages to respond to tumor cells in the CHT region. Upon engraftment of MDA-MB-231-B cells, we found an increase in macrophage number in the wt siblings at 2 and 4 dpi, compared to the uninjected condition, whereas no differences were found in macrophage number between injected and uninjected groups, in an *ody* background. The same conclusions were valid when macrophages were detected either by immunohistochemistry in the parental line *cxcr4b<sup>t26035</sup>* or as GFP expressing cells in the *cxcr4b<sup>t26035</sup> Tg(mpeg1:EGFP)<sup>g/22</sup>* line (Figure 7E-F).

To conclude, Cxcr4b signaling controls both macrophage and neutrophil responses to engrafted tumor cells in a zebrafish host, associated with the initiation of early metastatic events.

## Cxcr4b mutation affects gene expression of the *cxcl12* ligand and *mmp9*

In line with the impaired neutrophil motility in basal conditions and in response to cancer cells in the metastatic area, together with the affected recruitment of macrophages, we next hypothesized whether Cxcr4b mutation in the host could control the expression of the correspondent *cxcl12* ligands. We found that *cxcl12a*, described as the gene encoding the Cxcr4b ligand [39], was significantly reduced in *ody* compared to wt siblings under basal conditions (Figure 8A). Moreover, we quantified *cxcl12b* gene expression, as its redundant function in activating Cxcr4b signaling has been reported [27]. No significant difference but a trend towards reduced *cxcl12b* gene expression was observed in *ody* compared to wt siblings (Figure 8B). Similarly to *cxcl12a* and *cxcl12b*, the metalloprotease *mmp9* was found to be down regulated in *ody* larvae at 6 dpf (Figure 8C). Despite that *cxcr4b* expression is predominant in neutrophils and macrophages, it is not to be excluded that the expression in other cell types might be crucial in determining immune cell behavior under basal conditions as well as upon challenge by cancer cells, controlling gene expression of its own cognate ligands and

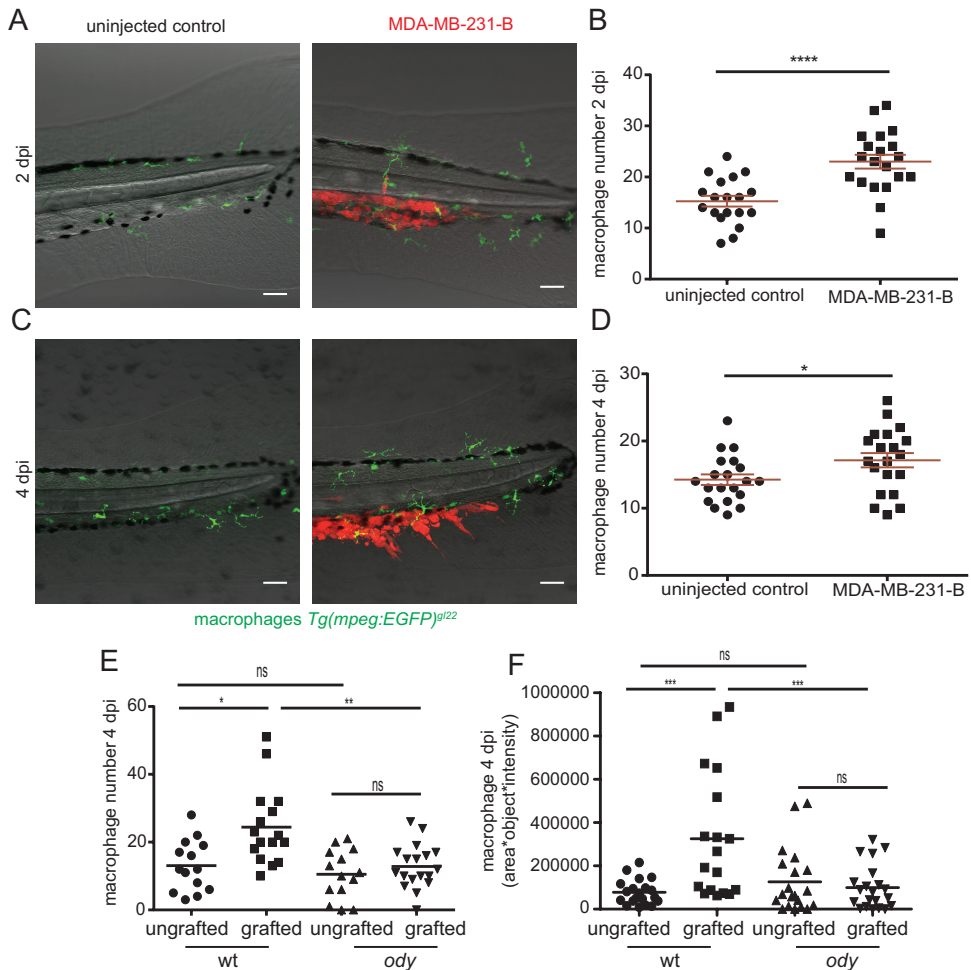


**Figure 7. Cancer cells fail to initiate early metastatic events and to trigger macrophage response in a *cxcr4* deficient host.** (A, B) Macrophages are recruited to the early metastatic site in 2 dpi *Tg(mpeg1:EGFP)<sup>g122</sup>* zebrafish larvae, engrafted with the breast cancer cell line MDA-MB-231-B DsRed. Compared to the uninjected control, an increased number of macrophages is found in the tail fin, in the surrounding of the secondary tumor mass, as shown in (A) and quantified in (B). Mann-Whitney test \*\*\*\* $p < 0.0001$ . Data are mean  $\pm$  SEM of two independent experiments (uninjected control:  $n=19$ , MDA-MB-231-B:  $n=20$ ). (C, D) Tumor cells establish an aggressive phenotype in the tail fin of 4 dpi zebrafish larvae, while surrounded by macrophages, as shown in the overlay in (C) and quantified in (D). Mann-Whitney test \* $p < 0.038$ . Data are mean  $\pm$  SEM of two independent experiments (uninjected control:  $n=20$ , MDA-MB-231-B:  $n=20$ ). Scale bars: 50  $\mu$ m. (E, F) The macrophage response to tumor cells at the metastatic site was assessed in *cxcr4b* mutants. (E) Macrophage numbers increase at the metastatic site when tumor cells are present in wt siblings, while the numbers do not change in the *ody* mutants at 4 dpi. In (E) macrophages are detected using immunohistochemistry (L-P<sup>+</sup>/TSA<sup>-</sup> cells) in the parental *cxcr4b<sup>t26035</sup>* line and quantified by manual counting during image analysis of each larva. Kruskal-Wallis, with Dunn's *post hoc* test. \* $p=0.014$ , \*\* $p=0.005$ , ns  $p > 0.05$  (wt, uninjected control:  $n=14$ ; wt, MDA-MB-231-B:  $n=16$ ; *ody*, uninjected:  $n=14$ ; *ody*, MDA-MB-231-B:  $n=18$ ). In (F) macrophages in the tail fin are *mpeg<sup>+</sup>* cells in the *cxcr4b<sup>t26035</sup> / Tg(mpeg1:EGFP)<sup>g122</sup>* line and quantification was based on the fluorescent signal by automated analysis in Image Pro, using

a macro written by H. de Bont (LACDR, Leiden University). One-way ANOVA, with Bonferroni *post hoc* test \*\*\* $p < 0.0001$ , ns  $p > 0.05$  (wt, uninjected control:  $n = 20$ ; wt, MDA-MB-231-B:  $n = 18$ ; *ody*, uninjected control:  $n = 20$ ; *ody*, MDA-MB-231-B:  $n = 21$ ). Micrographs of each larva used in the analyses were acquired with a Leica TCS SPE confocal microscope with a HC APO 20x DRY objective (0.7 N.A.). Macrophages were counted in the field of view.

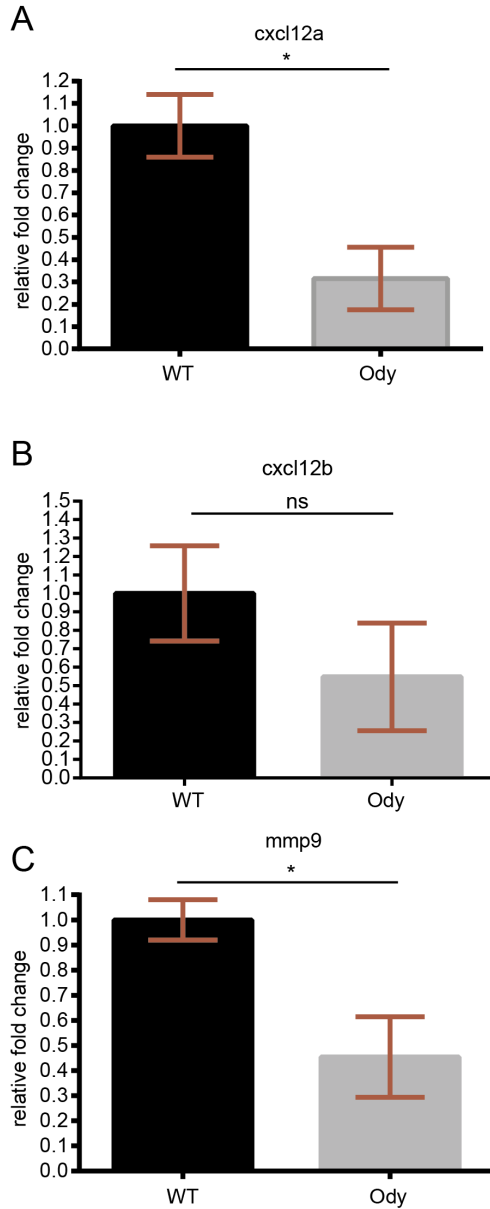


**Figure 8. Regulation of gene expression by *cxcr4b*.** Expression profiles of *cxcl12a* (A), *cxcl12b* (B) and *mmp9* (C) were quantified in the *ody* mutants compared to the wt siblings at 6 dpf. Un-paired t-test was used to assess significant differences (A) \* $p = 0.01$ , (B) ns=not significant, (C) \* $p = 0.02$ .

metalloproteases, required for cell motility.

### The transcriptomic signature of *Cxcr4b*-deficient neutrophils links to defective cellular motility

In our model, neutrophils are involved in the establishment of human tumor experimental metastases. We demonstrated that neutrophil motility is altered both under physiological condition (3 dpf zebrafish embryos) and in the presence of cancer cells in the metastatic region (4 dpi zebrafish larvae), when *Cxcr4b* signaling is impaired. In order to define the contribution of the neutrophilic *Cxcr4b* signaling axis in tumor cell invasion, RNA sequencing was performed from FACS-sorted GFP positive cells after dissociation of *cxcr4b*<sup>+/+</sup> and *cxcr4b*<sup>-/-</sup> *Tg (mpx:GFP)*<sup>i144</sup> 6 dpf larvae. Pathway analysis was performed in DAVID, after selecting 615 differentially expressed genes ( $p < 0.05$  in DESeq and edgeR) and converting them to human orthologues with gPROFILER. Genes involved in focal adhesion and ECM-receptor interaction were found up-regulated in neutrophils, together with genes involved in axon guidance, suggesting possible impairment in motility and tendency to have enhanced anchoring properties (Table 1). In particular, integrins are involved in adhesion strengthening and arrest of leukocytes on the endothelium, during transendothelial migration [40]. Laminin, fibronectin and collagen are components of the extracellular matrix and increased transcription levels suggest a tightening of the ECM and consequently challenged immune cell motility (Table 1). On the other hand, Tenascin XB, also belonging to the focal adhesion pathway, was found down-regulated. Members of the Roundabout signaling pathway (*slit1b*, *sema4gb* and *srgap1*), implicated among others in leukocyte chemotaxis and tumor angiogenesis [41] were found to be up-regulated. Subsequently, the pathway analysis was extended to differentially expressed genes identified through statistical analysis performed in RStudio using the package DESeq2 paired. Overall, the analysis performed in DESeq2 paired confirmed the enriched pathways identified with DESeq and edgeR. However, additional genes were identified, either belonging to previously described pathways (focal adhesion/ECM-Receptor interaction) or clustering in a new pathway (MAPK pathway) (Table 2). We also identified a key regulator of autophagy, *AMBRA-1* (autophagy/Beclin-1 regulator 1a), among the upregulated genes (Log2FoldChange=3.24 and  $p=0.0002$ ) in neutrophils isolated from the *ody* mutant. *AMBRA-1* is up-regulated upon autophagy and links with cell proliferation [42]. Furthermore, *NETRIN-1* (zebrafish *netrin-1b*), belonging to the family of laminin-secreted proteins and involved in neuronal chemotaxis [43, 44] and leukocyte migration [45], was found up-regulated in *cxcr4b*<sup>-/-</sup> neutrophils (Log2FoldChange=2.6 and  $p=0.00009$ ). *NETRIN-1* has previously been linked with reduced neutrophil and macrophage infiltration in a kidney injury model [46]. Down-regulated genes were found to cluster in the Metabolism of xenobiotics by cytochrome p450 pathway. Taken together, our sequencing data support the above described results that suggest motility alteration in neutrophils bearing a *cxcr4b* mutation.

**Table 1. Enriched pathways in *cxcr4b*<sup>-/-</sup> neutrophils (analysis performed with DESeq and edgeR)**

| Gene ID   | Gene symbol | Gene name  | DESeq    |         | edgeR |         |
|---|-------------|--|----------|---------|-------|---------|
|   |             |  | LogFC    | p       | LogFC | p       |
| <b>Focal adhesion/ECM-receptor interaction</b>      |             |  |          |         |       |         |
| ENSDARG00000056624                                  | figf        | c-fos induced growth factor                            | 3.9      | 3.0E-02 | 3.9   | 3.0E-02 |
| ENSDARG00000009014                                  | col11a1b    | collagen, type XI, alpha 1b                            | 1.8      | 6.0E-03 | 1.8   | 5.0E-03 |
| ENSDARG00000019815                                  | fn1a        | fibronectin 1a   | 1.9      | 3.0E-02 | 1.9   | 3.0E-02 |
| ENSDARG00000007950                                  | itga11b     | integrin, alpha 11b                                    | 4.8      | 3.0E-03 | 4.6   | 3.0E-03 |
| ENSDARG00000053232                                  | itgb1b.1    | integrin beta 1b.1                                     | 1.2      | 4.0E-02 | 1.2   | 4.0E-02 |
| ENSDARG000000102277                                 | lama1       | laminin, alpha 1                                       | 3.1      | 9.0E-03 | 3.1   | 1.0E-02 |
| ENSDARG00000099390                                  | lama2       | laminin, alpha 2                                       | 4        | 1.0E-02 | 3.9   | 2.0E-02 |
| ENSDARG00000018110                                  | pak4        | p21 protein (Cdc42/Rac)-activated kinase 4             | 1.5      | 2.0E-02 | 1.5   | 1.0E-02 |
| ENSDARG00000038139                                  | pdgfb       | platelet-derived growth factor beta polypeptide b      | 6.8      | 8.0E-04 | 6.3   | 6.0E-03 |
| ENSDARG00000078362                                  | tnc         | tenascin C   | 1.6      | 2.0E-02 | 1.6   | 3.0E-02 |
| <b>Axon guidance</b>                                |             |  |          |         |       |         |
| ENSDARG00000007461                                  | srgap1      | SLIT-ROBO Rho GTPase activating protein 1              | 2.9      | 4.0E-02 | 2.9   | 4.0E-02 |
| ENSDARG00000045064                                  | ablim1b     | actin binding LIM protein 1b                           | 1.3      | 2.0E-02 | 1.3   | 2.0E-02 |
| ENSDARG00000089790                                  | efna5a      | ephrin-A5a   | 2.8      | 1.0E-02 | 2.8   | 3.0E-02 |
| ENSDARG00000053232                                  | itgb1b.1    | integrin beta 1b.1                                     | 1.2      | 4.0E-02 | 1.2   | 4.0E-02 |
| ENSDARG00000022531                                  | ntn1b       | netrin 1b  | 2.6      | 9.0E-05 | 2.6   | 7.0E-03 |
| ENSDARG000000102556                                 | nfat5b      | nuclear factor of activated T-cells 5                  | 3.6      | 1.0E-02 | 3.5   | 2.6E-02 |
| ENSDARG00000076297                                  | nfatc3a     | nuclear factor of activated T-cells, cytoplasmic 3a    | 1.6      | 2.6E-02 | 1.6   | 3.2E-02 |
| ENSDARG00000018110                                  | pak4        | p21 protein (Cdc42/Rac)-activated kinase 4             | 1.5      | 2.2E-02 | 1.5   | 1.1E-02 |
| ENSDARG00000035132                                  | rgs3b       | regulator of G-protein signaling 3b                    | 2.3      | 3.0E-03 | 2.3   | 5.0E-03 |
| ENSDARG00000088143                                  | sema4gb     | semaphorin 4gb   | 1.00E+06 | 5.9E-04 | 7.9   | 4.5E-04 |
| ENSDARG00000099446                                  | slit1b      | slit homolog 1b  | 3.5      | 6.6E-03 | 3.5   | 2.3E-02 |
| <b>Metabolism of xenobiotics by cytochrome P450</b> |             |  |          |         |       |         |
| ENSDARG00000006220                                  | ugt1ab      | UDP glucuronosyltransferase 1 family a, b              | -2.6     | 4.9E-05 | -2.6  | 8.2E-03 |
| ENSDARG000000091211                                 | adh8a       | alcohol dehydrogenase 8a ]                             | -4.3     | 5.9E-03 | -4.2  | 4.6E-03 |
| ENSDARG00000098315                                  | cyp1a       | cytochrome P450, family 1, subfamily A                 | -4.1     | 1.1E-10 | -4.1  | 4.0E-03 |
| ENSDARG000000101423                                 | cyp2y3      | cytochrome P450, family 2, subfamily Y, polypeptide 3  | -1.5     | 1.8E-02 | -1.5  | 4.7E-02 |
| ENSDARG000000103295                                 | cyp3a65     | cytochrome P450, family 3, subfamily A, polypeptide 65 | -2.7     | 3.3E-06 | -2.7  | 4.5E-02 |
| ENSDARG00000039832                                  | zgc:173961  | zgc:173961 *   | -2.6     | 1.4E-05 | -2.6  | 1.0E-02 |
| ENSDARG00000090228                                  | gstal       | glutathione S-transferase                              | -2.7     | 1.1E-05 | -2.7  | 8.7E-03 |
| ENSDARG00000017388                                  | gstt1b      | glutathione S-transferase theta 1b                     | -2.8     | 1.9E-03 | -2.8  | 8.4E-03 |

**Table 2. Enriched pathways in *cxcr4b*<sup>-/-</sup> neutrophils (analysis performed with DESeq2 paired)**

| Gene ID  | Gene symbol | Gene name  | LogFC | p       |
|--|-------------|--|-------|---------|
| <b>Focal adhesion/ECM-receptor interaction</b> |             |  |       |         |
| ENSDARG00000032639                             | cd36        | CD36 molecule (thrombospondin receptor)                                    | -1.3  | 8.3E-03 |
| ENSDARG00000012405                             | col1a1a     | collagen, type I, alpha 1a   | 0.8   | 2.2E-02 |
| ENSDARG00000061436                             | col6a2      | collagen, type VI, alpha 2   | 1.0   | 4.5E-02 |
| ENSDARG00000074316                             | itga1       | integrin, alpha 1  | 1.1   | 8.8E-03 |
| ENSDARG000000103056                            | itga4       | integrin alpha 4   | 0.8   | 2.6E-02 |
| ENSDARG00000020785                             | lama4       | laminin, alpha 4   | 1.1   | 7.1E-03 |
| ENSDARG000000093572                            | lamc3       | laminin, gamma 3   | 1.5   | 5.2E-03 |
| ENSDARG00000060711                             | sv2bb       | synaptic vesicle glycoprotein 2Bb  | 1.7   | 3.4E-03 |
| ENSDARG00000008867                             | rap1b       | RAP1B, member of RAS oncogene family                                       | -0.9  | 2.1E-02 |
| ENSDARG00000007825                             | map2k1      | mitogen-activated protein kinase kinase 1                                  | -1.1  | 2.1E-02 |
| ENSDARG000000098578                            | pdgfab      | platelet-derived growth factor alpha polypeptide b                         | -1.0  | 2.1E-02 |
| <b>Cardiac muscle contraction</b>              |             |  |       |         |
| ENSDARG00000007739                             | atp1a1a.2   | ATPase, Na <sup>+</sup> /K <sup>+</sup> transporting, alpha 1a polypeptide | -1.6  | 5.8E-05 |
| ENSDARG00000018259                             | atp1a3a     | ATPase, Na <sup>+</sup> /K <sup>+</sup> transporting, alpha 3a polypeptide | 0.9   | 9.6E-03 |
| ENSDARG000000076833                            | atp1b1b     | ATPase, Na <sup>+</sup> /K <sup>+</sup> transporting, beta 1b polypeptide  | -1.5  | 4.0E-04 |
| ENSDARG000000063905                            | mt-co1      | cytochrome c oxidase I, mitochondrial                                      | -0.7  | 9.3E-03 |
| ENSDARG000000063908                            | mt-co2      | cytochrome c oxidase II, mitochondrial                                     | -0.6  | 4.1E-02 |
| ENSDARG000000063911                            | mt-atp6     | ATP synthase 6, mitochondrial  | -0.7  | 2.0E-02 |
| ENSDARG000000063912                            | mt-co3      | cytochrome c oxidase III, mitochondrial                                    | -0.7  | 1.7E-02 |
| ENSDARG000000023886                            | cacna2d4b   | calcium channel, voltage-dependent, alpha 2/delta subunit 4b               | 1.2   | 3.2E-02 |
| ENSDARG000000045230                            | cox6b1      | cytochrome c oxidase subunit VIb polypeptide 1                             | -1.2  | 4.2E-03 |
| ENSDARG000000038075                            | cyc1        | cytochrome c-1   | -0.7  | 1.9E-02 |
| ENSDARG000000079564                            | vmhc        | ventricular myosin heavy chain   | 2.1   | 3.7E-05 |
| <b>Axon guidance</b>                           |             |  |       |         |
| ENSDARG000000044029                            | efnb3a      | ephrin-B3a   | 1.2   | 3.2E-02 |
| <b>MAPK signaling pathway</b>                  |             |  |       |         |
| ENSDARG000000008867                            | rap1b       | RAP1B, member of RAS oncogene family                                       | -0.9  | 2.1E-02 |
| ENSDARG000000035535                            | rasa1a      | RAS p21 protein activator (GTPase activating protein) 1a                   | 0.8   | 4.5E-02 |
| ENSDARG000000005482                            | rapgef2     | Rap guanine nucleotide exchange factor (GEF) 2                             | 1.0   | 9.9E-03 |
| ENSDARG000000043241                            | arrrb1      | arrestin, beta 1   | 1.3   | 3.1E-02 |
| ENSDARG000000023886                            | cacna2d4b   | calcium channel, voltage-dependent, alpha 2/delta subunit 4b               | 1.2   | 3.2E-02 |
| ENSDARG000000102474                            | dusp16      | dual specificity phosphatase 16  | 1.4   | 9.6E-04 |
| ENSDARG000000061255                            | dusp3a      | dual specificity phosphatase 3a  | 1.4   | 1.5E-02 |
| ENSDARG000000009299                            | dusp8a      | dual specificity phosphatase 8a  | 1.0   | 3.0E-03 |
| ENSDARG000000092281                            | FLNB        | filamin B  | 1.3   | 2.1E-02 |
| ENSDARG000000007825                            | map2k1      | mitogen-activated protein kinase kinase 1                                  | -1.1  | 2.1E-02 |
| ENSDARG000000001234                            | map4k2      | mitogen-activated protein kinase kinase kinase kinase 2                    | -1.2  | 2.9E-02 |
| ENSDARG000000071357                            | map4k3b     | mitogen-activated protein kinase kinase kinase kinase 3b                   | 1.3   | 3.2E-03 |
| ENSDARG0000000070454                           | pla2g12a    | phospholipase A2, group XIIA   | -1.4  | 1.4E-02 |
| ENSDARG00000015662                             | pla2g12b    | phospholipase A2, group XIIB   | -1.4  | 1.4E-02 |
| ENSDARG000000098578                            | pdgfab      | platelet-derived growth factor alpha polypeptide b                         | -1.0  | 2.1E-02 |
| ENSDARG000000060551                            | rps6ka5     | ribosomal protein S6 kinase, polypeptide 5                                 | 1.5   | 8.7E-04 |
| ENSDARG000000017494                            | tgfbr1a     | transforming growth factor, beta receptor 1 a                              | 1.2   | 4.1E-02 |

**Table 1 and Table 2. Pathway analysis in *cxcr4b*-deficient neutrophils.** Genes selected with DESeq (p<0.05) and edgeR (p<0.05) analyses in RStudio (from 21621 to 615 genes) were converted to the human orthologues using g:Profiler and uploaded in DAVID Bioinformatics Resources 6.7 for pathway analysis. Up-regulation of genes involved in focal adhesion/ECM-Receptor interaction and axon guidance was identified, whereas down-regulation of genes in the metabolism of xenobiotic by P450 was found. Additional analysis was performed using DESeq2 paired (Table 2). The same pathways were identified with DESeq/edgeR (Table 1) and DESeq2 paired (Table 2) and the genes listed in Table 2 were in addition to genes described in

Table 1. Enriched pathways indicate alteration in motility, as shown by the analysis performed with DESeq and edgeR and reveal members of the MAPK signaling to be differentially expressed.

### **Transcriptome analysis suggests that *Cxcr4b* regulates motility and adhesion in macrophages**

Since we found that the recruitment of macrophages to the micrometastatic site is *Cxcr4b* dependent in our model, we also performed transcriptomic profiling of FACS-sorted macrophages from wt or *ody* mutant larvae. Pathway analysis was done on a list of 1231 genes selected after statistical analysis in DESeq and edgeR ( $p < 0.05$ ) and subsequently converted to human orthologues in gPROFILER. Approximately half of the candidate genes were found to be down-regulated in macrophages derived from *ody*, compared to the wt siblings. In the pathway analysis, these genes grouped in pathways regulating cell motility and adhesion, such as adherence junction, ECM-receptor interaction and actin cytoskeleton. Moreover, some members of the PI3K/AKT and STAT signaling pathways, known to be downstream of the CXCR4 in human were found to be down-regulated (Table 3). In addition, as performed for the analysis of the *cxcr4b* dependent transcriptomic signature in neutrophils, statistical analysis was done using the DESeq2 paired package in RStudio. From this analysis, more genes were found in previously identified pathways, whereas additional new pathways were also enriched. *cxcr4b* transcriptional control on the PI3K signaling pathway was confirmed, whereas genes involved in the cell cycle were found to be mostly up-regulated (Table 4). Importantly, some PI3K pathway members clustered in other pathways involved in cancer, including ErbB signaling, Insulin and mTOR signaling, as well as focal adhesion, regulation of actin cytoskeleton and leukocyte transendothelial migration. Taken together, the RNAseq analysis of macrophages supports that *Cxcr4b* controls gene expression of molecules generally activated after receptor stimulation by its own ligand and that *Cxcr4b* regulates signals involved in motility and adhesion.

### ***Cxcr4b* transcriptomic profiles reveal different signatures in neutrophils and macrophages**

A comparison between neutrophil and macrophage profiles was performed. An overall tendency towards upregulation was found in neutrophils from *ody* mutants (61% upregulated genes vs 39% downregulated genes) (Figure 9A) and partially in macrophages (51% upregulated genes vs 49% downregulated genes) (Figure 9B), when a cutoff was considered ( $p < 0.05$  in DESeq and edgeR). More in detail, in *ody* neutrophils 48% of the up-regulated genes showed an over 10-fold increase, whereas 57% of the down-regulated genes showed an over 10-fold decrease. In *ody* macrophages, a lower percentage of the differentially expressed genes showed such high fold changes. Instead, 59% of the up-regulated genes showed a fold change between 2 and 5, whereas 56% of the down-regulated genes showed a 2-to-5-fold decrease. Importantly, genes involved in focal adhesion, ECM-Receptor interaction and axon guidance were upregulated in *ody* neutrophils (Figure 9A), compared to wt, whereas other genes involved in adherens

**Table 3. Enriched pathways in *cxcr4b*-deficient macrophages (analysis performed with DESeq and edgeR)**

| Gene ID                                 | Gene symbol       | Gene name   | DESeq   |         | edgeR |         |
|---|-------------------|---|---------|---------|-------|---------|
|   |                   |   | LogFC   | p       | LogFC | p       |
| <b>Adherens junctions</b>               |                   |   |         |         |       |         |
| ENSDARG00000078888                      | iqgap1            | IQ motif containing GTPase activating protein 1                         | -1.50   | 1.6E-02 | -1.51 | 1.4E-03 |
| ENSDARG00000053235                      | lmo7b             | LIM domain 7b   | -4.98   | 1.7E-03 | -4.90 | 8.6E-03 |
| ENSDARG00000059466                      | wasf3a            | WAS protein family, member 3a   | 1.0E+06 | 6.0E-04 | 8.40  | 3.0E-03 |
| ENSDARG00000099786                      | ACTN4             | actinin, alpha 4  | -1.75   | 1.8E-03 | -1.77 | 2.6E-02 |
| ENSDARG00000018968                      | acvr1ba           | activin A receptor, type IBa  | -1.71   | 2.6E-02 | -1.72 | 1.2E-02 |
| ENSDARG000000104332                     | *si:dkey-173l11.3 | si:dkey-173l11.3  | -1.42   | 3.0E-02 | -1.43 | 3.3E-03 |
| ENSDARG00000078233                      | ctnnd1            | catenin (cadherin-associated protein), delta 1                          | -1.37   | 1.8E-02 | -1.39 | 2.5E-02 |
| ENSDARG00000071524                      | insrb             | insulin receptor b  | -3.09   | 8.0E-04 | -3.09 | 1.5E-04 |
| ENSDARG00000070903                      | met               | MET proto-oncogene, receptor tyrosine kinase                            | -6.19   | 1.7E-02 | -5.46 | 2.8E-03 |
| ENSDARG00000033042                      | ptprja            | protein tyrosine phosphatase, receptor type, J a                        | -1.82   | 9.1E-04 | -1.83 | 2.2E-04 |
| ENSDARG00000077506                      | tjp1a             | tight junction protein 1a   | 2.42    | 4.4E-02 | 2.40  | 3.8E-02 |
| ENSDARG00000038672                      | tcf7              | transcription factor 7 (T-cell specific, HMG-box)                       | -4.36   | 3.6E-02 | -4.06 | 1.3E-02 |
| ENSDARG00000026294                      | erbB2             | erb-b2 receptor tyrosine kinase 2                                       | -7.44   | 1.4E-04 | -6.73 | 8.5E-04 |
| <b>ECM-Receptor interaction</b>         |                   |   |         |         |       |         |
| ENSDARG00000079388                      | agrn              | Agtrin  | 6.59    | 1.1E-03 | 6.41  | 6.2E-04 |
| ENSDARG00000069093                      | col2a1a           | collagen, type II, alpha 1a   | -2.48   | 2.8E-03 | -2.48 | 1.7E-03 |
| ENSDARG00000016153                      | dag1              | dystroglycan 1  | -1.75   | 4.2E-02 | -1.77 | 2.8E-02 |
| ENSDARG00000076564                      | hspg2             | heparan sulfate proteoglycan 2  | 3.97    | 1.2E-03 | 3.92  | 1.2E-03 |
| ENSDARG000000103056                     | itga4             | integrin alpha 4  | -1.51   | 1.4E-02 | -1.52 | 2.7E-03 |
| ENSDARG00000006314                      | itgav             | integrin, alpha V   | -1.31   | 3.5E-02 | -1.32 | 5.3E-03 |
| ENSDARG00000053232                      | itgb1b.1          | integrin, beta 1b.1   | -1.81   | 2.2E-02 | -1.83 | 9.0E-03 |
| ENSDARG00000012942                      | itgb5             | integrin, beta 5  | -3.04   | 8.1E-03 | -3.06 | 8.6E-03 |
| ENSDARG00000044318                      | itgb7             | integrin, beta 7  | -1.16   | 4.9E-02 | -1.18 | 2.4E-02 |
| ENSDARG00000036279                      | lamc1             | laminin, gamma 1  | -3.97   | 3.4E-03 | -3.92 | 1.6E-02 |
| ENSDARG00000010785                      | thbs1b            | thrombospondin 1b   | -4.80   | 1.3E-03 | -4.64 | 2.1E-03 |
| <b>Regulation of actin cytoskeleton</b> |                   |   |         |         |       |         |
| ENSDARG00000078888                      | iqgap1            | IQ motif containing GTPase activating protein 1                         | -1.50   | 1.6E-02 | -1.51 | 1.4E-03 |
| ENSDARG00000078430                      | tiam1a            | T-cell lymphoma invasion and metastasis 1a                              | -1.18   | 2.6E-02 | -1.20 | 2.4E-02 |
| ENSDARG00000099786                      | ACTN4             | actinin, alpha 4  | -1.75   | 1.8E-03 | -1.77 | 2.6E-02 |
| ENSDARG00000036375                      | cyfip2            | cytoplasmic FMR1 interacting protein 2                                  | -1.15   | 3.5E-02 | -1.17 | 3.9E-02 |
| ENSDARG00000032049                      | enah              | enabled homolog (Drosophila)  | 2.39    | 1.7E-02 | 2.37  | 2.9E-02 |
| ENSDARG00000037924                      | gna13b            | guanine nucleotide binding protein (G protein), alpha 13b               | -1.88   | 5.2E-03 | -1.89 | 1.9E-04 |
| ENSDARG000000103056                     | itga4             | integrin alpha 4  | -1.51   | 1.4E-02 | -1.52 | 2.7E-03 |
| ENSDARG00000096587                      | itgam             | integrin, alpha M (complement component 3 receptor 3 subunit)           | -3.58   | 1.1E-03 | -3.57 | 1.8E-04 |
| ENSDARG00000053232                      | itgb1b.1          | integrin, beta 1b.1   | -1.81   | 2.2E-02 | -1.83 | 9.0E-03 |
| ENSDARG00000012942                      | itgb5             | integrin, beta 5  | -3.04   | 8.1E-03 | -3.06 | 8.6E-03 |
| ENSDARG00000044318                      | itgb7             | integrin, beta 7  | -1.16   | 4.9E-02 | -1.18 | 2.4E-02 |
| ENSDARG00000002589                      | mylpfb            | myosin light chain, phosphorylatable, fast skeletal muscle b            | 2.24    | 2.9E-03 | 2.23  | 3.3E-02 |
| ENSDARG00000001014                      | myh9b             | myosin, heavy chain 9b, non-muscle                                      | -2.48   | 2.2E-05 | -2.50 | 2.1E-06 |
| ENSDARG000000100396                     | pip5k1aa          | phosphatidylinositol-4-phosphate 5-kinase, type I, alpha, a             | -3.24   | 6.1E-04 | -3.21 | 9.9E-05 |
| ENSDARG00000075456                      | pik3ca            | phosphatidylinositol-4,5-bisphosphate 3-kinase, catalytic subunit alpha | -1.98   | 3.6E-02 | -1.98 | 2.6E-02 |
| ENSDARG00000017757                      | pik3cg            | phosphatidylinositol-4,5-bisphosphate 3-kinase, catalytic subunit gamma | -1.07   | 2.7E-02 | -1.09 | 3.6E-02 |
| ENSDARG00000017661                      | braf              | B-Raf proto-oncogene, serine/threonine kinase                           | -2.34   | 1.8E-02 | -2.33 | 1.3E-02 |

\*zebrafish orthologue to human CDH1, cadherin type 1

Table continues on next page

| Acute myeloid leukemia |         |  |       |         |       |         |
|------------------------|---------|--|-------|---------|-------|---------|
| ENSDARG00000075456     | pik3ca  | phosphatidylinositol-4,5-bisphosphate 3-kinase, catalytic subunit alpha          | -1.98 | 3.6E-02 | -1.98 | 2.6E-02 |
| ENSDARG00000017757     | pik3cg  | phosphatidylinositol-4,5-bisphosphate 3-kinase, catalytic subunit gamma          | -1.07 | 2.7E-02 | -1.09 | 3.6E-02 |
| ENSDARG00000003680     | runx1t1 | runx-related transcription factor 1; translocated to, 1 (cyclin D-related)       | 4.77  | 1.9E-02 | 4.56  | 7.6E-03 |
| ENSDARG00000022712     | stat3   | signal transducer and activator of transcription 3 (acute phase response factor) | -1.18 | 4.8E-02 | -1.19 | 1.6E-02 |
| ENSDARG00000055588     | stat5b  | signal transducer and activator of transcription 5b                              | -2.09 | 2.5E-02 | -2.08 | 7.5E-03 |
| ENSDARG000000038672    | tcf7    | transcription factor 7 (T-cell specific, HMG-box)                                | -4.36 | 3.6E-02 | -4.06 | 1.3E-02 |
| ENSDARG00000099657     | akt1    | v-akt murine thymoma viral oncogene homolog 1                                    | -1.79 | 1.9E-02 | -1.80 | 1.2E-02 |
| ENSDARG00000104810     | akt3a   | v-akt murine thymoma viral oncogene homolog 3a                                   | -2.38 | 2.1E-02 | -2.37 | 1.1E-02 |
| ENSDARG00000017661     | braf    | B-Raf proto-oncogene, serine/threonine kinase                                    | -2.34 | 1.8E-02 | -2.33 | 1.3E-02 |

Table 4. Enriched pathways in *cxcr4b*<sup>-/-</sup> macrophages (analysis performed with DESeq2 paired)

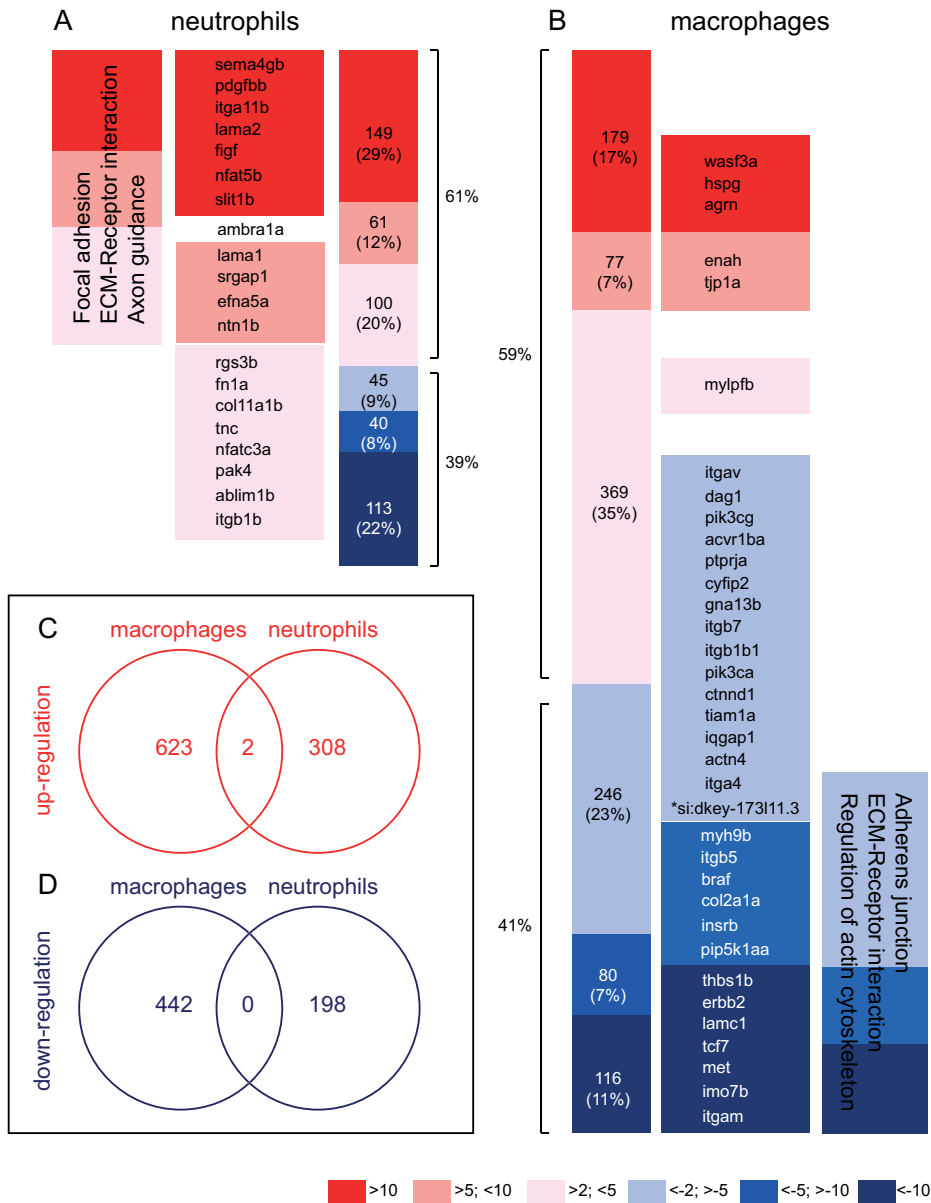
| Gene ID                          | Gene symbol | Gene name   | DESeq2 paired |          |
|----------------------------------|-------------|---|---------------|----------|
|                                  |             |   | LogFC         | p        |
| Adherens junction                |             |   |               |          |
| ENSDARG00000076486               | acp1        | acid phosphatase 1, soluble                                   | 0.88          | 3.92E-02 |
| ENSDARG00000104332               |             | si:dkey-173l11.3  | -1.28         | 4.37E-04 |
| ENSDARG00000007923               | ptpn1       | protein tyrosine phosphatase, non-receptor type 1             | -0.70         | 3.51E-02 |
| ENSDARG00000103435               | sorbs1      | sorbin and SH3 domain containing 1                            | 1.35          | 9.93E-03 |
| ENSDARG00000098695               | VCL         | vinculin  | -1.29         | 7.44E-03 |
| Regulation of actin cytoskeleton |             |   |               |          |
| ENSDARG00000025826               | gna12a      | guanine nucleotide binding protein (G protein) alpha 12a      | -1.01         | 1.44E-02 |
| ENSDARG00000103467               | limk1a      | LIM domain kinase 1a  | -1.21         | 4.77E-03 |
| ENSDARG00000025826               | gna12a      | guanine nucleotide binding protein (G protein) alpha 12a      | -1.01         | 1.44E-02 |
| ENSDARG00000037917               | itga3a      | integrin, alpha 3a  | -1.68         | 3.47E-03 |
| ENSDARG00000006314               | itgav       | integrin, alpha V   | -1.20         | 3.49E-04 |
| ENSDARG00000028222               | itgb8       | integrin, beta 8  | -1.11         | 4.90E-02 |
| ENSDARG00000068918               | map2k2b     | mitogen-activated protein kinase kinase 2b                    | -1.20         | 2.35E-02 |
| ENSDARG00000063295               | myh9a       | myosin, heavy chain 9a, non-muscle                            | -0.80         | 9.48E-03 |
| ENSDARG00000038524               | pik3r1      | phosphoinositide-3-kinase, regulatory subunit 1 (alpha)       | -0.66         | 3.74E-02 |
| ENSDARG00000102762               | pik3r5      | phosphoinositide-3-kinase, regulatory subunit 5               | -0.94         | 2.83E-02 |
| ENSDARG00000036252               | rras2       | related RAS viral (r-ras) oncogene homolog 2                  | -1.31         | 1.28E-02 |
| ENSDARG00000098695               | VCL         | vinculin  | -1.29         | 7.44E-03 |
| Focal adhesion                   |             |   |               |          |
| ENSDARG00000018285               | pdpk1b      | 3-phosphoinositide dependent protein kinase 1b                | -0.87         | 1.84E-02 |
| ENSDARG00000054937               | badb        | BCL2-associated agonist of cell death b                       | 1.13          | 3.90E-03 |
| ENSDARG00000075437               | shc1        | SHC (Src homology 2 domain containing) transforming protein 1 | -0.98         | 6.63E-03 |
| ENSDARG00000017803               | gsk3b       | glycogen synthase kinase 3 beta                               | -1.32         | 2.71E-04 |
| ENSDARG00000037917               | itga3a      | integrin, alpha 3a  | -1.68         | 3.47E-03 |
| ENSDARG00000028222               | itgb8       | integrin, beta 8  | -1.11         | 4.90E-02 |
| ENSDARG00000056964               | ilk         | integrin-linked kinase  | -0.95         | 1.08E-02 |
| ENSDARG00000070903               | met         | MET proto-oncogene, receptor tyrosine kinase                  | -1.32         | 3.03E-02 |
| ENSDARG00000002589               | mylfb       | myosin light chain, phosphorylatable, fast skeletal muscle b  | 1.63          | 7.39E-03 |

Table continues on next page

| Leukocyte transendothelial migration |          |   |       |          |
|--------------------------------------|----------|---|-------|----------|
| ENSDARG00000022841                   | ptk2ba   | protein tyrosine kinase 2 beta, a                                       | -1.18 | 5.75E-03 |
| ENSDARG00000099786                   | ACTN4    | actinin, alpha 4  | -1.69 | 1.35E-03 |
| ENSDARG00000078233                   | ctnnd1   | catenin (cadherin-associated protein), delta 1                          | -1.31 | 1.93E-03 |
| ENSDARG00000057633                   | cxcr4a   | chemokine (C-X-C motif) receptor 4a                                     | 1.60  | 3.93E-03 |
| ENSDARG00000018283                   | cyba     | cytochrome b-245, alpha polypeptide                                     | 0.68  | 4.27E-02 |
| ENSDARG00000056615                   | cybb     | cytochrome b-245, beta polypeptide (chronic granulomatous disease)      | -0.74 | 1.38E-02 |
| ENSDARG000000103056                  | itga4    | integrin alpha 4  | -1.38 | 4.71E-05 |
| ENSDARG00000053232                   | itgb1b.1 | integrin, beta 1b.1   | -1.54 | 1.91E-03 |
| ENSDARG00000042816                   | mmp9     | matrix metalloproteinase 9  | -0.65 | 4.12E-02 |
| ENSDARG00000002589                   | mylpfb   | myosin light chain, phosphorylatable, fast skeletal muscle b            | 1.63  | 7.39E-03 |
| ENSDARG00000075456                   | pik3ca   | phosphatidylinositol-4,5-bisphosphate 3-kinase, catalytic subunit alpha | -1.45 | 1.33E-02 |
| ENSDARG00000017757                   | pik3cg   | phosphatidylinositol-4,5-bisphosphate 3-kinase, catalytic subunit gamma | -1.11 | 1.73E-03 |
| ENSDARG00000038524                   | pik3r1   | phosphoinositide-3-kinase, regulatory subunit 1 (alpha)                 | -0.66 | 3.74E-02 |
| ENSDARG000000102762                  | pik3r5   | phosphoinositide-3-kinase, regulatory subunit 5                         | -0.94 | 2.83E-02 |
| ENSDARG00000022254                   | prkcbb   | protein kinase C, beta b  | -1.03 | 4.62E-03 |
| ENSDARG00000076697                   | SIPA1    | signal-induced proliferation-associated 1                               | -0.83 | 3.87E-02 |
| Phosphatidylinositol signaling       |          |   |       |          |
| ENSDARG00000076025                   | dgkzb    | diacylglycerol kinase, zeta b   | -1.15 | 7.10E-03 |
| ENSDARG00000003446                   | ippk     | inositol 1,3,4,5,6-pentakisphosphate 2-kinase                           | -1.16 | 1.45E-02 |
| ENSDARG00000011909                   | itpr2    | inositol 1,4,5-trisphosphate receptor, type 2                           | -1.02 | 1.22E-02 |
| ENSDARG00000063352                   | inpp4aa  | inositol polyphosphate-4-phosphatase, type Ia                           | -2.17 | 1.36E-07 |
| ENSDARG00000078106                   | ocrl     | oculocerebrorenal syndrome of Lowe                                      | -1.16 | 2.94E-03 |
| ENSDARG000000100396                  | pip5k1aa | phosphatidylinositol-4-phosphate 5-kinase, type I, alpha, a             | -2.61 | 1.60E-06 |
| ENSDARG00000075456                   | pik3ca   | phosphatidylinositol-4,5-bisphosphate 3-kinase, catalytic subunit alpha | -1.45 | 1.33E-02 |
| ENSDARG00000017757                   | pik3cg   | phosphatidylinositol-4,5-bisphosphate 3-kinase, catalytic subunit gamma | -1.11 | 1.73E-03 |
| ENSDARG00000038524                   | pik3r1   | phosphoinositide-3-kinase, regulatory subunit 1 (alpha)                 | -0.66 | 3.74E-02 |
| ENSDARG000000102762                  | pik3r5   | phosphoinositide-3-kinase, regulatory subunit 5                         | -0.94 | 2.83E-02 |
| ENSDARG00000068763                   | plcg2    | phospholipase C, gamma 2  | -0.74 | 4.24E-02 |
| ENSDARG00000022254                   | prkcbb   | protein kinase C, beta b  | -1.03 | 4.62E-03 |
| ENSDARG00000025011                   | synj1    | synaptojanin 1  | -0.95 | 4.25E-02 |

**Table 3 and Table 4. Pathway analysis in *cxcr4b*-null macrophages.** RNA sequencing of FACS-sorted macrophages was analyzed using DESeq and edgeR in RStudio. A gene list was generated based on statistically significant difference ( $p < 0.05$ ) in mean expression (3 replicates) comparing wt and *cxcr4b*  $-/-$  populations (from 19259 to 1231 genes). The list of selected zebrafish genes was converted into the human orthologue list in g:Profiler. Pathway analysis was then performed in DAVID Bioinformatics Resources 6.7. Enriched genes clustered in the adherens junction, ECM-receptor interaction, regulation of actin cytoskeleton and acute myeloid leukemia pathways. Most of the identified genes in these pathways were down-regulated (Table 3). Analysis performed with DESeq2 paired showed similar pathways identified with DESeq and edgeR analyses, suggesting *Cxcr4b*-dependent control of macrophage motility and adhesion. Additionally, members of the PI3K signaling pathway were found to be down-regulated, whereas most of cell cycle-related genes were up-regulated (Table 4). The same pathways were identified with DESeq/edgeR (Table 3) and DESeq2 paired (Table 4) and the genes listed in Table 4 are additional to the genes described in Table 3.

junction, ECM-Receptor interaction and actin cytoskeleton were downregulated in *ody* macrophages, compared to wt (Figure 9B). These observations suggest that *Cxcr4b* controls cell adhesion and migration processes in neutrophils and macrophages in a different manner. In addition, we looked at how many genes were commonly up- or down-regulated in *Cxcr4b*-deficient neutrophils and macrophages. Interestingly, there were only two commonly up-regulated genes (FC, fold change > 2,  $p < 0.05$ ) [*megf6* (multiple EGF-like-domains 6) and *rcan 3*, regulator of calcineurin 3] and no commonly down-regulated genes (FC < 0.5,  $p < 0.05$ ), showing that neutrophils and macrophages display a markedly different *Cxcr4b*-dependent gene expression signature (Figure 9C, D).



**Figure 9. Up- and down-regulated genes in *Cxcr4b*-deficient or wt neutrophils and macrophages.** (A) Heatmap showing up- and down-regulated genes in *cxcr4b*<sup>-/-</sup> neutrophils compared to *cxcr4b*<sup>+/+</sup> neutrophils. 61% is the percentage of up-regulated genes, whereas 39% is the percentage of down-regulated genes. Genes involved in focal adhesion, ECM-Receptor interaction and axon guidance are up-regulated. *ambra1a* is involved in autophagy. (B) Heatmap showing up- and down-regulated genes in *cxcr4b*<sup>-/-</sup> macrophages compared to *cxcr4b*<sup>+/+</sup> macrophages. 59% is the percentage of up-regulated genes, whereas 41% is the percentage of down-regulated genes. Genes involved in adherens junction, ECM-Receptor interaction and regulation of actin cytoskeleton are down-regulated (with the exception of *myl9b*, *tjp1a*, *enah*, *agr*, *hspg* and *wasf3a*, which are up-regulated genes in these same pathways). Percentages of up- or down-regulation are calculated based on the total number of genes left after a cutoff of  $p < 0.05$  in both DESeq and edgeR

(neutrophil dataset: from  $n=21517$  to  $n=508$ , macrophage dataset: from  $n=19095$  to  $n=1067$ ). Before the analysis, 107 genes were manually removed in the neutrophil dataset due to high variation among the triplicates and 164 were manually removed in the macrophage dataset due to high variation among the triplicates. An alternative analysis method using DESeq2 paired confirmed the affected pathways (Table 2). (C, D) Up- and down-regulated genes in neutrophils and macrophages are shown in the Venn diagrams, obtained using the web tool available at <http://bioinformatics.psb.ugent.be/webtools/Venn/>. Almost none of the genes selected with a cutoff of  $p<0.05$  in both DESeq and edgeR are commonly (C) up- or (D) down-regulated in neutrophils and macrophages.

## Discussion

Chemokines are key mediators of directional cell migration and the CXCR4-CXCL12 chemokine axis is well known to display major roles in tumor progression, guiding tumor cell homing to CXCL12 expressing organs [47]. Consequently, targeting the CXCR4 receptor expressed by cancer cells is a pharmacological approach that is currently explored in the clinic to limit tumor spreading and metastases [48]. At the same time, it is important to consider the effect of CXCR4 signaling on the tumor microenvironment, especially in view of the antagonizing or supportive functions that myeloid cells are known to have on tumor progression [49]. We previously showed that the zebrafish xenograft model is a powerful tool to study tumor-microenvironment interactions as CXCR4-based interspecies cross talk takes place (previous chapter). Moreover, the role of neutrophils in preparing the metastatic niche has been previously described by our group [22]. We found that the non-pathological migration correlate with tumor cell invasion in the caudal hematopoietic tissue (CHT), functionally analogous to the fetal liver in mammalian embryo development. Hence, we hypothesized the involvement of CXCR4 signaling in controlling neutrophil motility and immune-tumor cell interactions involved in the initiation of early metastatic events and micrometastasis formation. First, we found that in zebrafish larvae neutrophils and macrophages express high levels of *cxcr4b*, the homologue of human CXCR4 and paralogue of zebrafish *cxcr4a*. Then, we used a *cxcr4b* homozygote mutant zebrafish (also known as *odysseus* or *ody*) and showed that engrafted human tumor cells failed to form micrometastases in the CHT region. Therefore, myeloid cell impairment or a non-functional Cxcr4b signaling led to experimental tumor micrometastasis inhibition.

Investigating a potential role of the host Cxcr4b signaling in the formation of early metastasis by affecting immune cell motility was the next approach. Interestingly, we found that neutrophil motility was reduced in *cxcr4b-null* zebrafish embryos, prior to engraftment with human cancer cells at the same time point considered by [22] to link neutrophil physiological migration to tumor invasion in the tail fin. Importantly, we next investigated whether Cxcr4b signaling affects neutrophil development. In mammals, CXCR4 and CXCR2 chemokine signaling axes regulate hematopoietic stem cell (HSC) retention in and mobilization from the bone marrow, respectively [19, 21]. CXCR4 chemical inhibition upon AMD3100 treatment results in mobilized HSCs [50]. Furthermore, patients affected by WHIM syndrome, characterized by neutropenia and enhanced susceptibility to infection, bear a CXCR4-gain-of-function mutation that causes

neutrophil retention in hematopoietic sites, in response to cognate ligand CXCL12, highly expressed in the bone marrow [51]. These findings have been confirmed in a zebrafish model of WHIM syndrome, where neutrophils expressing constitutive active *cxc4b* were retained in the CHT and mobilized only upon *cxc12a* knock down [28]. We found that the number of neutrophils in the CHT in the *ody* mutants was higher than in the wt siblings at 2 dpf. Because the overall neutrophil number was not affected by the *cxc4b* mutation, a higher number of neutrophils in the CHT surprisingly suggested enhanced neutrophil retention. These findings show that receptor stimulation by cognate ligand is needed to activate cell motility, despite of chemotaxis. Retention and reduced motility of neutrophils with impaired Cxcr4b signaling at 2 and 3 dpf, respectively, support the hypothesis that neutrophil physiological behavior plays an important role in cancer micrometastasis formation at early stages. In our model indeed, tumor cell engraftment is performed in 2 dpf zebrafish embryos and between 0 and 1 dpi (3 dpf embryos), tumor cells adapt to the host microenvironment, possibly preparing micrometastasis occurrence.

We next investigated if neutrophils played an important role in preparing the metastatic niche in later stages of tumor micrometastasis formation, when tumor cell invasion has largely taken place. Therefore, neutrophil number was counted in 6 dpf zebrafish larvae and, in contrast to the observations at 2 dpf, a reduction in neutrophils localized in the CHT was found in *ody* mutants, with tendency towards a reduced overall number in a whole larva. We hypothesize that the dichotomy in neutrophil numbers is linked to the role of CXCR4 signaling during hematopoiesis. Using the zebrafish embryo model, it has recently been shown that HSPCs colonize the hematopoietic tissue, interacting with mesenchymal cells and inducing modification in the perivascular niche. In the same study, the mesenchymal cells express *cxc12a*, whereas *cxc4b* expression is mainly found in the CHT region and treatment with the CXCR4 antagonist AMD3100 reduced the number of *runx*<sup>+</sup> hematopoietic progenitors [32]. In line with their findings, we propose that the reduced number of neutrophils in the CHT of 6 dpf *ody* larvae relates to the reduced number of HSPCs and suggest that further investigations should be carried on to confirm this hypothesis. Importantly, a lower number of neutrophils in the CHT in 6 dpf *ody* mutants might result in a reduced niche modification due to a lower number of paths traced into the collagen by neutrophils themselves. On the other end, the increased number of neutrophils in earlier stages suggests the potential role of Cxcr4b in the primitive wave of hematopoiesis.

After investigating physiological neutrophil development and motility, we then unraveled neutrophil behavior in the presence of engrafted tumor cells, able to initiate early metastatic events. An acute response to engrafted cancer cells into the blood circulation of 2 dpf zebrafish embryos resulted in no alteration in Cxc4b-deficient neutrophils. To assess the neutrophil acute response, the number of *mpx*<sup>+</sup> cells was counted in the CHT of zebrafish embryos few hours after tumor cell inoculation. As neutrophil numbers were decreased in the CHT of engrafted wt or *ody* embryos, we

propose that neutrophils leave the CHT, mounting an acute response towards danger signals, in line with previous observations of demand-driven granulopoiesis upon bacterial infection [38]. Moreover, this response is independent from *cxcr4b*. On the other hand, an altered response was found at later stages. In 6 dpf (4 dpi) zebrafish larvae, tumor cells have established a secondary tumor mass and initiated local tissue invasion. In response, wt siblings diminished the number of neutrophils in the CHT, probably increasing their mobilization in order to begin a response towards nearby cancer cells. Mobilized neutrophils were found to migrate and move in the surrounding of metastasizing cancer cells, with a tendency to slow down and interact with human malignant cells. In contrast, *cxcr4b* deficient neutrophils remained in the CHT and failed to localize in the surrounding of the tumor micrometastases in the tail fin of zebrafish larvae, suggesting a possibly diminished inflammatory response.

In agreement with the altered response of neutrophils to tumor engraftments, the neutrophilic *cxcr4b* transcriptomic signature revealed enhanced adhesive properties, due to upregulation of the integrins, as well as increased interaction with the ECM and alteration of the cytoskeleton reorganization. Members of the Roundabout signaling pathway were also differentially expressed. Roundabout signaling is associated with axon guidance mechanisms and its role in cancer metastasis has been reported [52]. Importantly, *slit1b*, found up-regulated in *ody*, functions as a repellent molecule that interferes with leukocyte chemotaxis [53] and specifically blocks the ability of circulating neutrophils to migrate directionally [54]. Moreover, we propose *NETRIN-1* as a candidate gene that links neutrophil ability to provide trophic signals to cancer cells. *NETRIN-1* indeed has been reported to reduce neutrophil infiltration in ischemic acute kidney injury by inhibiting COX-2 and PGE<sub>2</sub> production [46]. PGE<sub>2</sub> has been identified as a possible trophic signal that sustains neoplastic transformation in a zebrafish transgenic model of cancer [55].

In this work, we also investigated the role of Cxcr4b in the response of macrophages towards engrafted tumor cells. In our *in vivo* model, zebrafish macrophages accumulate in the surrounding of human cancer cells forming micrometastases in the tail fin region, around the hematopoietic tissue. A severe reduction of this response in *ody* mutants suggests that Cxcr4b signaling affects macrophage accumulation in tissues infiltrated by cancer cells. Interestingly, the triple negative breast cancer cell line MDA-MB-231-B expresses nearly undetectable levels of *CXCL12* (as shown in Chapter 4), suggesting therefore that Cxcr4b-dependent macrophage recruitment is guided by zebrafish cognate Cxcl12. In line with this hypothesis, the expression levels of zebrafish *cxcl12* chemokines (significant reduction in *cxcl12a* and tendency to reduction in *cxcl12b*) were found reduced in the *ody* mutants at 6 dpf. Although we recently showed that macrophage number and motility in *ody* are not altered (Chapter 4), further investigations are needed to provide a better understanding of the *cxcr4b* role in macrophage development and response to malignant cells.

In this study we identified the *cxcr4b* transcriptomic signature in macrophages that have not been challenged by tumor cells. This revealed a down-regulation of genes involved in actin cytoskeleton reorganization, interaction with the ECM, focal adhesion, adherens junctions, and trans-endothelial migration, together suggesting impaired motility and adhesive properties. Moreover, as expected, members belonging to the PI3K/AKT and STAT pathways, downstream in the CXCR4 signaling cascade, were found to be down-regulated in *Cxcr4b*-deficient macrophages. This result suggests that despite that CXCR4 regulates downstream molecules on a protein level, it elicits regulatory functions of the same targets also on mRNA level. Importantly, the comparison of the *cxcr4b* transcriptomic profile in neutrophils and macrophages revealed that an overall tendency towards gene upregulation could be found. However, almost no differentially expressed genes in one of the myeloid cell population were shared by the other class of phagocytes. Specifically, genes involved in cell migration and adhesion were up-regulated in neutrophils and down-regulated in macrophages sorted from *ody* mutants. Therefore, the transcriptional signatures indicate that CXCR4 signaling controls adhesive and migratory properties by different mechanisms in macrophages and neutrophils.

The *cxcr4b* gene is highly expressed in macrophages and recent evidence suggests CXCR4 as M2-type marker [10]. M2 macrophages are involved in tissue homeostasis and take part in tissue remodeling after injury and inflammation, participating in angiogenesis [56]. M2 macrophages are suggested to support cancer proliferation and relapse after chemotherapy [10]. Therefore, further investigations are needed to gain more understanding over *Cxcr4b* signaling function in the macrophage contribution to tumor development. Generally, the transcriptomic profile of neutrophils and macrophages challenged by cancer cells, in the context of *cxcr4b* mutation, will provide further clues on myeloid subtype shifts during malignant progression. In conclusion, we demonstrate that CXCR4 signaling plays a major role in the innate immune response to early metastatic events and contributes to the establishment of tumor micrometastases. The development of CXCR4-targeted therapies directed to the tumor microenvironment is therefore essential.

## Materials and Methods

### Zebrafish husbandry

Zebrafish lines were kept in compliance with the local animal welfare regulations and European directives. Zebrafish adults were maintained according to standard protocols (zfin.org), in a 10/14 hour dark/light cycle. Embryos were maintained at 28°C in Egg water (60 µg/ml Ocean salt in distilled water), containing 0.003% PTU (1-phenyl-2-thiourea) to block pigmentation.

## Zebrafish lines

Zebrafish reporter lines used in this study were *Tg(mpx:GFP)<sup>i114</sup>* [26], *Tg(mpeg1:EGFP)<sup>gl22</sup>* [57], *Tg(Kdrl:EGFP)<sup>s843</sup>* [58]. The *cxcr4b<sup>t26035</sup>* line [29] was outcrossed with each reporter line mentioned above. Homozygote *cxcr4b<sup>-/-</sup>* mutant embryos (*odysseus* or *ody*) were distinguished from wild type *cxcr4b<sup>+/+</sup>* and heterozygote *cxcr4b<sup>+/-</sup>* siblings by phenotype (incomplete lateral line deposition) and genotype identification. Genotyping of adult fish by KASP assay was performed using the following primers A1 (reverse) 5'-TGACGGTGGTCTTCAGTGCCTT-3', A2 (reverse) 5'-TGACGGTGGTCTTCAGTGCCTA-3' and C1 (forward) 5'-CAAGAACTCCAAGGGTCAGACTCTA-3' and confirmed by sequencing using previously described primers [39].

## Cell culture

Breast MDA-MB-231-B dsRed (kindly provided by P. ten Dijke and Y. Drabsch, LUMC, Leiden, The Netherlands), MDA-MB-157 mCherry (ATCC®) and prostate PC3-M-Pro4-Luc2 (mCherry or tdTomato) (kindly provided by G. van der Pluijm, LUMC, Leiden, The Netherlands) cancer cell lines were cultured in DMEM medium complemented with 10% fetal calf serum (FCS), at 37°C in a humidified atmosphere with 5% CO<sub>2</sub>. Cell lines were regularly tested for mycoplasma with Universal Mycoplasma Detection kit (30-1012k, ATCC).

## Pu.1 knock down

Pu.1 (Spi1b, 1 mM) and standard control morpholino injections (0.1 mM) were performed to deplete neutrophils and macrophages as previously described [22]. Morpholino efficiency was assessed by counting number of Mpx<sup>+</sup> neutrophils in the *Tg(mpx:GFP)<sup>i114</sup>* zebrafish line.

## Xenograft experiments

Tumor cells were inoculated in the blood circulation of 2 day post fertilization (dpf) zebrafish embryos as previously described (Chapter 3).

## Tumor burden

Zebrafish embryos engrafted with fluorescently labelled tumor cells were screened for correct engraftment 5-6 hours after inoculation into the blood circulation at 2 dpf, using a Leica MZ16FA fluorescent microscope coupled to a DFC420C camera. Larvae were positioned on a Petri dish with 1.5% agarose coating and tumor burden was quantified at 4 dpi, acquiring monographs of the metastatic site, in the CHT region. LAS AF Lite software was used to overlay the GFP and dsRed channels and snapshots were analyzed in Image-Pro Analyzer 7.0 (Media Cybernetics). For each larva tumor burden was calculated based on number of objects multiplied by mean area and mean intensity, generated with a macro designed by H.de Bont (Toxicology, LACDR, Leiden University)

and previously used to quantify tumor migration and proliferation [59, 60].

### Neutrophil number and motility

Neutrophil number was quantified by manual counting, using a Leica MZ16FA fluorescent microscope. Neutrophil basal motility was assessed using a Leica TCS SPE confocal microscope with a HC APO 20x DRY objective (0.7 N.A.). 3 dpf larvae were mounted on a 1% low melting point agarose layer, containing tricaine and covering the glass surface of a Will-Co Dish® (Pelco®, Ted Pella, Inc). Egg water containing anesthetic was added on top of each larva. Timelapse was performed for 30 minutes, with 1 minute intervals. Maximum projections were generated, tail movements were corrected using Stack Reg plugin and neutrophil tracking was performed using the Manual Tracking plugin in ImageJ-Fiji [61]. Neutrophil motility in response to metastatic cancer cells was quantified with a Nikon A1 confocal laser scanning microscope (Tokyo, Japan) using the 488 and 561 laser lines with 20x (NA 0.75) lens. Images were acquired every minute during timelapse. Videos were analyzed using NIS-Elements AR and tracking performed for the first 30 frames in ImageJ, with Manual Tracking plugin.

### Macrophage quantification

Macrophages were identified as GFP<sup>+</sup> cells in the *Tg(mpeg1:EGFP)<sup>g122</sup>* zebrafish line or as L-Plastin<sup>+</sup>/mpx<sup>-</sup> in the parental *cxc4b<sup>t30516</sup>* line. Immunohistochemistry was performed as previously described (Chapter 3). Macrophage number in the metastatic region was quantified both by manual and automated methods. For automated analysis performed on *Tg(mpeg1:EGFP)<sup>g122</sup>*, the Image-Pro Analyzer 7.0 (Media Cybernetics) software was used, in combination with the same macro employed to calculate tumor burden. Number of objects multiplied by mean area and mean intensity were used to delineate cell shape and quantify number of macrophages present in the field of view.

### RNA isolation and real-time PCR

Expression levels of *cxcl12a*, *cxcl12b* and *mmp9* were quantified in 6 dpf *cxc4b<sup>t26035</sup>* *Tg(Kdr1:EGFP)<sup>s843</sup>* larvae. RNA was isolated using TRIZOL extraction method, according to the manufacturer's instruction from a pool of zebrafish larvae (10<n<15). DNase treatment was performed using RQ1 RNase free-DNase (M6101 Promega). 1 µg input RNA was used for cDNA synthesis (i-Script™ cDNA synthesis kit, Bio-Rad). Expression levels were measured by real-time PCR (iQ™ SYBR® Green Supermix, Bio-Rad), using the Chromo4™ Four-Color Real-Time PCR system. Relative fold changes of gene expression were calculated using the  $\Delta\Delta C_t$  method. The following primers were used: *mmp9* forward 5'CATTAAAGATGCCCTGATGTATCCC-3' and *mmp9* reverse 5'-AGTGGTGGTCCGTGGTTGAG-3' [62]; *cxcl12a* forward 5'-GCTGGTGCCGTCCACAGTCA-3' and *cxcl12a* reverse 5'-GGGGCAGTTGGTGTGTGGAG-3'; *cxcl12b* forward 5'-TGCTGGTGTGCTCCACCCT-3' and *cxcl12b* reverse 5' -TGGAAAGGGCAGCTGGGAGTGT-3'. Peptidylprolyl isomerase A-like (*prial*) was used as housekeeping gene (forward 5'- ACACTGAAACACGGAGGCAAAG -3'

and reverse RV 5'-CATCCACAACCTTCCCGAACAC-3'). *cxcl12a*, *cxcl12b* and *ppial* primers were kindly provided by Chao Cui (Leiden University).

### Myeloid *cxcr4b* transcriptomic signature: from larval dissociation to RNA sequencing analysis

Zebrafish lines *cxcr4b*<sup>t26035</sup> *Tg(mpx:GFP)*<sup>114</sup> and *cxcr4b* t26035 *Tg(mpeg1:EGFP)*<sup>9122</sup> were used to isolate neutrophils and macrophages, respectively, from 6 dpf larvae. After harvesting, eggs were kept in Petri dishes (n≤100) at 28.5°C to allow synchronized embryo development. Triplicates of GFP positive embryos (100-150 per replicate) were selected for dissociation, performed according to [63]. Dissociation with 0.4 mg/ml collagenase/DPBS (Liberase TL, Roche, #05401020001) was alternatively used. Larvae were transferred directly from Egg water to collagenase solution. Dissociation was obtained mechanically with pipetting and 2 incubation steps at 28.5°C for 10 min. 10% FCS was added and sample preparation was continued as described in [63]. Sorting was performed with a BD FACSAria™ III Cell Sorter (BD Biosciences, San Jose, CA, USA) with the BD FACSDiva software (version 6.1.3) and gates defined using GFP negative larvae. After sorting, samples were stored in QIAzol at -80°C. RNA isolation was performed using miRNeasy Mini kit (# 217004 Qiagen). On-column DNase digestion was performed, using RNase-Free DNase Set (# 79254 Qiagen). Agilent Bioanalyzer 2100, RNA 6000 Pico kit (Agilent, Santa Clara) was used to assess RNA quality. cDNA synthesis and amplification were performed with SMARTer® Ultra™ Low Input RNA Kit for Sequencing - v3 (Clontech) and cDNA quality validated, using Agilent 2100 BioAnalyzer and the High Sensitivity DNA Chip from Agilent's High Sensitivity DNA Kit (#5067-4626, Agilent). cDNA shearing, library preparation and validation, and Illumina sequencing (HiSeq 2000) were performed as described in [63] by ZF-SCREENS (Leiden, The Netherlands). Reads (18.684.327 is an average of 12 samples) were mapped to Ensembl transcripts (GRCz10.80) and statistical analysis based on negative binomial distribution performed in R Studio, using DESeq, DESeq2 paired and EdgeR packages, available at Bioconductor.org. Pathway analysis was performed using DAVID Bioinformatics Resources 6.7. Identification of *cxcr4a* and *cxcr4b* expression levels in neutrophils and macrophages by RNA sequencing shown in Figure 2 was performed as described in [63].

### Statistics

Statistically significant difference was assessed using GraphPad Prism (versions 5.0 and 6.0). Un-paired t-test was used in datasets of two groups and Welch's correction applied when group variances were significantly different (p<0.05). One-way ANOVA with Bonferroni *post hoc* test was used in datasets of three or more groups (continuous variable), while Kruskal-Wallis with Dunn's *post hoc* test was used to estimate significant difference in the case of counts (discrete variable).

## Author contributions

CT and CS performed experiments and data analysis. VT contributed to immune cell sorting, optimization of RNA sequencing analytical methods and scientific discussions. AHM gave valuable suggestions on data analysis and experimental design. CT and BESJ designed experiments and wrote the manuscript. All authors approved the final version of this manuscript.

## Acknowledgments

The authors would like to acknowledge Arwin Groenewoud (Leiden University) for scientific discussion, Tomasz Prajsnar (Leiden University) for helping with cell sorting and RNA sequencing analysis and Lanpeng Chen (Leiden University) for PC3-Pro4-Luc engraftments. The authors are grateful to Zakia Kanwal and Julien Rougeot for the initial RNA sequencing analysis of *cxcr4a/b* expression levels on FACS-sorted neutrophils and macrophages. The authors acknowledge all members of the fish care team and D. Gilmour (EMBL, Heidelberg) and H. Knaut (Max-Planck-Institute, Tübingen) for providing the *cxcr4b*<sup>t26035</sup> zebrafish line.

## Funding

The present work was supported by the Netherlands Organization for Scientific Research (NWO) (TOP GO Grant: 854.10.012). VT was supported by the European Marie-Curie Initial Training Network FishForPharma (PITN-GA-2011-289209).

## References

1. Quail, D.F. and J.A. Joyce, Microenvironmental regulation of tumor progression and metastasis. *Nat Med*, 2013. 19(11): p. 1423-37.
2. Hanahan, D. and R.A. Weinberg, Hallmarks of Cancer: The Next Generation. *Cell*, 2011. 144(5): p. 646-674.
3. Guo, F., et al., CXCL12/CXCR4: a symbiotic bridge linking cancer cells and their stromal neighbors in oncogenic communication networks. *Oncogene*, 2015.
4. Janowski, M., Functional diversity of SDF-1 splicing variants. *Cell Adhesion & Migration*, 2009. 3(3): p. 243-249.
5. Duda, D.G., et al., CXCL12 (SDF1alpha)-CXCR4/CXCR7 pathway inhibition: an emerging sensitizer for anticancer therapies? *Clin Cancer Res*, 2011. 17(8): p. 2074-80.
6. Feig, C., et al., Targeting CXCL12 from FAP-expressing carcinoma-associated fibroblasts synergizes with anti-PD-L1 immunotherapy in pancreatic cancer. *Proc Natl Acad Sci U S A*, 2013. 110(50): p. 20212-7.
7. Biswas, S.K. and A. Mantovani, Macrophage plasticity and interaction with lymphocyte

subsets: cancer as a paradigm. *Nature Immunology*, 2010. 11(10): p. 889-896.

8. De Palma, M. and C.E. Lewis, Macrophage regulation of tumor responses to anticancer therapies. *Cancer Cell*, 2013. 23(3): p. 277-86.
9. Roussos, E.T., J.S. Condeelis, and A. Patsialou, Chemotaxis in cancer. *Nature Reviews Cancer*, 2011. 11(8): p. 573-587.
10. Hughes, R., et al., Perivascular M2 Macrophages Stimulate Tumor Relapse after Chemotherapy. *Cancer Res*, 2015. 75(17): p. 3479-91.
11. Allavena, P., et al., The Yin-Yang of tumor-associated macrophages in neoplastic progression and immune surveillance. *Immunological Reviews*, 2008. 222: p. 155-161.
12. Fridlender, Z.G., et al., Polarization of Tumor-Associated Neutrophil Phenotype by TGF-beta: "N1" versus "N2" TAN. *Cancer Cell*, 2009. 16(3): p. 183-194.
13. Piccard, H., R.J. Muschel, and G. Opdenakker, On the dual roles and polarized phenotypes of neutrophils in tumor development and progression. *Critical Reviews in Oncology Hematology*, 2012. 82(3): p. 296-309.
14. Rivera, L.B., et al., Intratumoral Myeloid Cells Regulate Responsiveness and Resistance to Antiangiogenic Therapy. *Cell Reports*, 2015. 11(4): p. 577-591.
15. Silva, M.T., When two is better than one: macrophages and neutrophils work in concert in innate immunity as complementary and cooperative partners of a myeloid phagocyte system. *Journal of Leukocyte Biology*, 2010. 87(1): p. 93-106.
16. Kim, N.D. and A.D. Luster, The role of tissue resident cells in neutrophil recruitment. *Trends Immunol.*, 2015. 36(9): p. 547-55.
17. Casanova-Acebes, M., et al., Innate immune cells as homeostatic regulators of the hematopoietic niche. *International Journal of Hematology*, 2014. 99(6): p. 685-694.
18. Shiozawa, Y., et al. Bone marrow as a metastatic niche for disseminated tumor cells from solid tumors. *Bonekey Rep.*, 2015. 4, DOI: 10.1038/bonekey.2015.57.
19. Eash, K.J., et al., CXCR2 and CXCR4 antagonistically regulate neutrophil trafficking from murine bone marrow. *Journal of Clinical Investigation*, 2010. 120(7): p. 2423-2431.
20. Eash, K.J., et al., CXCR4 is a key regulator of neutrophil release from the bone marrow under basal and stress granulopoiesis conditions. *Blood*, 2009. 113(19): p. 4711-4719.
21. Martin, C., et al., Chemokines acting via CXCR2 and CXCR4 control the release of neutrophils from the bone marrow and their return following senescence. *Immunity*, 2003. 19(4): p. 583-593.
22. He, S.N., et al., Neutrophil-mediated experimental metastasis is enhanced by VEGFR inhibition in a zebrafish xenograft model. *Journal of Pathology*, 2012. 227(4): p. 431-445.
23. Murayama, E., et al., Tracing hematopoietic precursor migration to successive hematopoietic organs during zebrafish development. *Immunity*, 2006. 25(6): p. 963-975.

24. Wetterwald, A., et al., Optical Imaging of cancer metastasis to bone marrow - A mouse model of minimal residual disease. *American Journal of Pathology*, 2002. 160(3): p. 1143-1153.
25. Page, D.M., et al., An evolutionarily conserved program of B-cell development and activation in zebrafish. *Blood*, 2013. 122(8): p. e1-11.
26. Renshaw, S.A., et al., A transgenic zebrafish model of neutrophilic inflammation. *Blood*, 2006. 108(13): p. 3976-8.
27. Bussmann, J. and E. Raz, Chemokine-guided cell migration and motility in zebrafish development. *Embo Journal*, 2015. 34(10): p. 1309-1318.
28. Walters, K.B., et al., Live imaging of neutrophil motility in a zebrafish model of WHIM syndrome. *Blood*, 2010. 116(15): p. 2803-11.
29. Knaut, H., et al., A zebrafish homologue of the chemokine receptor Cxcr4 is a germ-cell guidance receptor. *Nature*, 2003. 421(6920): p. 279-282.
30. Kawai, T. and H.L. Malech, WHIM syndrome: congenital immune deficiency disease. *Curr Opin Hematol*, 2009. 16(1): p. 20-6.
31. Chen, A.T. and L.I. Zon, Zebrafish blood stem cells. *J Cell Biochem*, 2009. 108(1): p. 35-42.
32. Tamplin, O.J., et al., Hematopoietic stem cell arrival triggers dynamic remodeling of the perivascular niche. *Cell*, 2015. 160(1-2): p. 241-52.
33. Boettcher, S. and M.G. Manz, Sensing and translation of pathogen signals into demand-adapted myelopoiesis. *Curr Opin Hematol*, 2016. 23(1): p. 5-10.
34. Manz, M.G. and S. Boettcher, Emergency granulopoiesis. *Nat Rev Immunol*, 2014. 14(5): p. 302-14.
35. Takizawa, H., S. Boettcher, and M.G. Manz, Demand-adapted regulation of early hematopoiesis in infection and inflammation. *Blood*, 2012. 119(13): p. 2991-3002.
36. Wirths, S., S. Bugl, and H.G. Kopp, Neutrophil homeostasis and its regulation by danger signaling. *Blood*, 2014. 123(23): p. 3563-6.
37. Liongue, C., et al., Zebrafish granulocyte colony-stimulating factor receptor signaling promotes myelopoiesis and myeloid cell migration. *Blood*, 2009. 113(11): p. 2535-46.
38. Hall, C.J., et al., Infection-responsive expansion of the hematopoietic stem and progenitor cell compartment in zebrafish is dependent upon inducible nitric oxide. *Cell Stem Cell*, 2012. 10(2): p. 198-209.
39. Miyasaka, N., H. Knaut, and Y. Yoshihara, Cxcl12/Cxcr4 chemokine signaling is required for placode assembly and sensory axon pathfinding in the zebrafish olfactory system. *Development*, 2007. 134(13): p. 2459-68.
40. Mitroulis, I., et al., Leukocyte integrins: role in leukocyte recruitment and as therapeutic targets in inflammatory disease. *Pharmacol Ther*, 2015. 147: p. 123-35.

41. Legg, J.A., et al., Slits and Roundabouts in cancer, tumour angiogenesis and endothelial cell migration. *Angiogenesis*, 2008. 11(1): p. 13-21.
42. Cianfanelli, V., M. D'Orazio, and F. Cecconi, AMBRA1 and BECLIN 1 interplay in the crosstalk between autophagy and cell proliferation. *Cell Cycle*, 2015. 14(7): p. 959-63.
43. Dupin, I., et al., Subrepellent doses of Slit1 promote Netrin-1 chemotactic responses in subsets of axons. *Neural Dev*, 2015. 10: p. 5.
44. Round, J. and E. Stein, Netrin signaling leading to directed growth cone steering. *Curr Opin Neurobiol*, 2007. 17(1): p. 15-21.
45. Ly, N.P., et al., Netrin-1 inhibits leukocyte migration in vitro and in vivo. *Proc Natl Acad Sci U S A*, 2005. 102(41): p. 14729-34.
46. Ranganathan, P.V., et al., Netrin-1 regulates the inflammatory response of neutrophils and macrophages, and suppresses ischemic acute kidney injury by inhibiting COX-2-mediated PGE2 production. *Kidney Int*, 2013. 83(6): p. 1087-98.
47. Vandercappellen, J., J. Van Damme, and S. Struyf, The role of CXC chemokines and their receptors in cancer. *Cancer Lett*, 2008. 267(2): p. 226-44.
48. Scala, S., *Molecular Pathways: Targeting the CXCR4-CXCL12 Axis-Untapped Potential in the Tumor Microenvironment*. *Clin Cancer Res*, 2015.
49. Galdiero, M.R., et al., Tumor associated macrophages and neutrophils in cancer. *Immunobiology*, 2013. 218(11): p. 1402-10.
50. Kessans, M.R., M.L. Gatesman, and D.R. Kockler, Plerixafor: a peripheral blood stem cell mobilizer. *Pharmacotherapy*, 2010. 30(5): p. 485-92.
51. Gulino, A.V., WHIM syndrome: a genetic disorder of leukocyte trafficking. *Curr Opin Allergy Clin Immunol*, 2003. 3(6): p. 443-50.
52. Ballard, M.S. and L. Hinck, A roundabout way to cancer. *Adv Cancer Res*, 2012. 114: p. 187-235.
53. Wu, J.Y., et al., The neuronal repellent Slit inhibits leukocyte chemotaxis induced by chemotactic factors. *Nature*, 2001. 410(6831): p. 948-52.
54. Tole, S., et al., The axonal repellent, Slit2, inhibits directional migration of circulating neutrophils. *J Leukoc Biol*, 2009. 86(6): p. 1403-15.
55. Feng, Y., S. Renshaw, and P. Martin, Live imaging of tumor initiation in zebrafish larvae reveals a trophic role for leukocyte-derived PGE(2). *Curr Biol*, 2012. 22(13): p. 1253-9.
56. Mantovani, A. and A. Sica, Macrophages, innate immunity and cancer: balance, tolerance, and diversity. *Curr Opin Immunol*, 2010. 22(2): p. 231-7.
57. Ellett, F., et al., mpeg1 promoter transgenes direct macrophage-lineage expression in zebrafish. *Blood*, 2011. 117(4): p. e49-56.
58. Jin, S.W., et al., Cellular and molecular analyses of vascular tube and lumen formation

in zebrafish. *Development*, 2005. 132(23): p. 5199-209.

59. Ghotra, V.P.S., et al., Automated Whole Animal Bio-Imaging Assay for Human Cancer Dissemination. *Plos One*, 2012. 7(2).

60. van der Ent, W., et al., Ewing sarcoma inhibition by disruption of EWSR1-FLI1 transcriptional activity and reactivation of p53. *Journal of Pathology*, 2014. 233(4): p. 415-424.

61. Schneider, C.A., W.S. Rasband, and K.W. Eliceiri, NIH Image to ImageJ: 25 years of image analysis. *Nat Methods*, 2012. 9(7): p. 671-5.

62. van der Vaart, M., et al., The DNA damage-regulated autophagy modulator DRAM1 links mycobacterial recognition via TLP-MYD88 to autophagic defense. *Cell Host Microbe*, 2014. 15(6): p. 753-67.

63. Rougeot, J., et al., RNA sequencing of FACS-sorted immune cell populations from zebrafish infection models to identify cell specific responses to intracellular pathogens. *Methods Mol Biol*, 2014. 1197: p. 261-74.

